Monthly Notices
of the
ROYAL ASTRONOMICAL SOCIETY

MNRAS **490,** 718–732 (2019)
Advance Access publication 2019 September 16

doi:10.1093/mnras/stz2585

Supernovae and their host galaxies – VI. Normal Type Ia and 91bg-like supernovae in ellipticals

L. V. Barkhudaryan [1]★ A. A. Hakobyan [1]★ A. G. Karapetyan [1] G. A. Mamon [2] D. Kunth,[2] V. Adibekyan[3] and M. Turatto[4]

[1]*Byurakan Astrophysical Observatory, 0213 Byurakan, Aragatsotn Province, Armenia*
[2]*Institut d'Astrophysique de Paris, Sorbonne Universités, UPMC Univ Paris 6 et CNRS, UMR 7095, 98 bis bd Arago, F-75014 Paris, France*
[3]*Instituto de Astrofísica e Ciência do Espaço, Universidade do Porto, CAUP, Rua das Estrelas, P-4150-762 Porto, Portugal*
[4]*INAF – Osservatorio Astronomico di Padova, Vicolo dell'Osservatorio 5, I-35122 Padova, Italy*

Accepted 2019 September 5. Received 2019 August 14; in original form 2019 June 13

ABSTRACT

We present an analysis of the galactocentric distributions of the 'normal' and peculiar '91bg-like' subclasses of 109 supernovae (SNe) Ia, and study the global parameters of their elliptical hosts. The galactocentric distributions of the SN subclasses are consistent with each other and with the radial light distribution of host stellar populations, when excluding bias against central SNe. Among the global parameters, only the distributions of $u - r$ colours and ages are inconsistent significantly between the ellipticals of different SN Ia subclasses: the normal SN hosts are on average bluer/younger than those of 91bg-like SNe. In the colour–mass diagram, the tail of colour distribution of normal SN hosts stretches into the Green Valley – transitional state of galaxy evolution, while the same tail of 91bg-like SN hosts barely reaches that region. Therefore, the bluer/younger ellipticals might have more residual star formation that gives rise to younger 'prompt' progenitors, resulting in normal SNe Ia with shorter delay times. The redder and older ellipticals that already exhausted their gas for star formation may produce significantly less normal SNe with shorter delay times, outnumbered by 'delayed' 91bg-like events. The host ages (lower age limit of the delay times) of 91bg-like SNe does not extend down to the stellar ages that produce significant u-band fluxes – the 91bg-like events have no prompt progenitors. Our results favour SN Ia progenitor models such as He-ignited violent mergers that have the potential to explain the observed SN/host properties.

Key words: supernovae: individual: Type Ia – galaxies: abundances – galaxies: elliptical and lenticular, cD – galaxies: evolution – galaxies: star formation – galaxies: stellar content.

1 INTRODUCTION

The most energetic and relatively uniform class among supernovae (SNe) explosions are Type Ia SNe that were used to discover the accelerating expansion of the Universe (e.g. Riess et al. 1998; Perlmutter et al. 1999). It is widely accepted that Type Ia SN arises from a thermonuclear explosion of a carbon–oxygen (CO) white dwarf (WD) in an interacting binary stellar system. In short, the most favoured are single degenerate (SD; Nomoto, Iwamoto & Kishimoto 1997) and double degenerate (DD; Iben & Tutukov 1984) progenitor scenarios. In the SD scenario, a CO WD accretes material from a main-sequence/subgiant star, or a red giant star, or even a helium star, causing the WD mass to reach the Chandrasekhar mass limit ($\approx 1.4\,M_{\odot}$) and explode. In the DD scenario, a double WD system loses orbital angular momentum due to gravitational wave emission, leading to coalescence/accretion and explosion. Recent results suggest that both scenarios are possible (see e.g. Maeda & Terada 2016, for a review on various progenitor models).

The fortune of SNe Ia in cosmology is due to the fact that despite their moderate inhomogeneity, they are the best standardizable candles in the Universe due to a correlation between their luminosity at maximum light and the shape of the light curve (LC), with faster declining objects being fainter (first proposed by Rust 1974 and Pskovskii 1977). This is known as the width–luminosity relation of SN LC (Phillips 1993). In addition, the LC decline rates Δm_{15}, i.e. the difference in magnitudes between the maximum and 15 d after the maximum light, and colours of SNe Ia are related: the faster declining LCs correspond to the intrinsically redder events (e.g. Riess et al. 1998; Phillips et al. 1999). The luminosity of an SN Ia and the Δm_{15} depend on the kinetic energy of the explosion, the mass of radioactive ^{56}Ni in the ejecta and opacity (e.g. Arnett 1982; Mazzali et al. 2007).

Despite the relatively uniform maximum luminosities of Type Ia SNe, there is increasing evidence for photometric and spectroscopic

★ E-mail: barkhudaryan@bao.sci.am (LVB); hakobyan@bao.sci.am (AAH)

diversities among them. In comparison with the observational properties of normal SNe Ia (Branch, Fisher & Nugent 1993), specialists in the field often refer to two 'traditional' and most common subclasses of peculiar SNe Ia – overluminous '91T-like' events with slower declining LCs (Filippenko et al. 1992b; Phillips et al. 1992; Ruiz-Lapuente et al. 1992) and subluminous '91bg-like' SNe with faster declining LCs (Filippenko et al. 1992a; Leibundgut et al. 1993; Turatto et al. 1996). These peculiar SNe Ia make up a considerable fraction of local Type Ia SNe (e.g. Li et al. 2011a, ∼30 per cent), and are of crucial importance for understanding SNe Ia events in general. A few per cent of other subclasses of peculiar SNe Ia include the faint but slowly declining '02es-like' SNe, '02cx-like' events with low luminosities (also called SNe Iax), 'Ca-rich' transients, the extremely luminous so-called 'super-Chandrasekhar' (also called '06gz-like') SNe, and SNe Ia showing circumstellar medium interactions (see e.g. Taubenberger 2017, for a recent review on most of the extremes of Type Ia SNe).

When considering only the most populated subclasses of SNe Ia, i.e. normal, 91T-, and 91bg-like events, the lower mass of the host galaxy (the later morphological type or higher the specific star formation rate, SFR), the brighter and slower the SNe Ia that are exploded, on average (e.g. Hamuy et al. 1996; Howell 2001; Gallagher et al. 2005; Neill et al. 2009; González-Gaitán et al. 2011, 2014; Li et al. 2011a). 91T-like SNe occur in star-forming host galaxies, while such an object has never been discovered in elliptical galaxies (e.g. Howell 2001; Gallagher et al. 2005; Li et al. 2011a), where the stellar population almost always consists of old stars. 91bg-like events prefer host galaxies with elliptical and lenticular morphologies (E–S0), sometimes they explode also in early-type spirals (e.g. Howell 2001; Li et al. 2011a). Normal SNe Ia are discovered in host galaxies with any morphologies from ellipticals to late-type spirals (e.g. Li et al. 2011a).

In the literature, there are many efforts in studying the links between the spectral as well as LC properties of SNe Ia and the global as well as local properties at SN explosion sites of their host galaxies, such as mass, colour, SFR, metallicity, and age of the stellar population (e.g. Hamuy et al. 2000; Ivanov, Hamuy & Pinto 2000; Gallagher et al. 2005, 2008; Howell et al. 2009; Neill et al. 2009; Sullivan et al. 2010; Gupta et al. 2011; Galbany et al. 2012; Pan et al. 2014, 2015; Anderson et al. 2015; Moreno-Raya et al. 2016; Kim et al. 2018; Rose, Garnavich & Berg 2019). In such studies, SNe Ia host galaxies with various morphological properties, e.g. old ellipticals with spherically distributed stellar content, lenticulars with an old stellar population in a huge spherical bulge plus a prominent exponential disc, and spirals with old bulge and young star-forming disc components are simultaneously included in the samples. In this case, it is difficult to precisely analyse the spatial distribution of SNe, and associate them with a concrete stellar component (bulge or thick/thin discs, old, or intermediate/young) in the hosts due to different or unknown projection effects (e.g. Hakobyan et al. 2016, 2017). In addition, E–S0 and spiral host galaxies have had different evolutionary paths through major/minor galaxy–galaxy interaction (e.g. Kaviraj et al. 2009; McIntosh et al. 2014; Schawinski et al. 2014), and therefore this important aspect should be clearly distinguished.

In this study, we morphologically select from the Sloan Digital Sky Survey (SDSS) only elliptical host galaxies of SNe Ia, which are known to have the simplest structural properties of the composition in comparison with lenticular and spiral galaxies (e.g. Kormendy et al. 2009). As already mentioned, in these galaxies no 91T-like events have been discovered, they mostly host normal and 91bg-like SNe (e.g. Howell 2001). Therefore, these two subclasses of Type Ia SNe are the subject of study in this paper.[1]

Recall that the 91bg-like SNe are unusually red and have peak luminosities that are 2 ± 0.5 mag lower than normal SNe Ia (the typical peak magnitude of normal SNe Ia is $M_B \simeq -19.1$ mag, see Taubenberger et al. 2008 and references therein). They have faster declining LCs $1.8 \lesssim \Delta m_{15} \lesssim 2.1$, compared with $\Delta m_{15} \lesssim 1.7$ for normal events, and their ejecta velocities are small at any epoch in comparison with normal SNe Ia (e.g. Benetti et al. 2005; Wang et al. 2013). In the post-maximum spectra, particularly notable is the presence of unusually strong O I λ 7774 and Ti II absorption lines. Despite the recent detection of strong H α in the nebular spectrum of ASASSN-18tb (a 91bg-like event; Kollmeier et al. 2019), there is no evidence that fast declining SNe are more likely to have late time H α emission (Sand et al. 2019). For more details of the spectra and LC properties of 91bg-like events, the reader is referred to a review by Taubenberger (2017).

The explosion mechanism, which should explain the main characteristics of these events, including the low ^{56}Ni masses, is still under debate. The DD scenario, the helium layer detonation triggered sub-Chandrasekhar mass explosion, and the scenario of collision of two WDs are competing (e.g. Hillebrandt & Niemeyer 2000; Mazzali & Hachinger 2012; Pakmor et al. 2013; Dong et al. 2015; Crocker et al. 2017).

In the earlier literature, several attempts have been done to study the projected radial and surface density distributions of nearby SNe Ia in morphologically selected elliptical host galaxies (Guseinov, Kasumov & Kalinin 1980; Bartunov, Makarova & Tsvetkov 1992; Tsvetkov, Pavlyuk & Bartunov 2004; Förster & Schawinski 2008). These studies showed that, in general, the distribution of Type Ia SNe is consistent with the light (de Vaucouleurs) profile of their elliptical host galaxies, which are dominated by old and metal-rich stellar populations (e.g. González Delgado et al. 2015). However, mainly because of the lack of the spectral and LC data, these studies did not separate the normal and 91bg-like subclasses. For the first time, Pavlyuk & Tsvetkov (2016) attempted to compare the surface density distributions of the subclasses of nearby SNe Ia, in particular for those of the normal and 91bg-like events. However, the morphological types of SN hosts were not limited to elliptical galaxies only, thus mixing different progenitor populations from bulges and discs (see also Gallagher et al. 2008; Panther et al. 2019).

On the other hand, Gallagher et al. (2008) studied optical absorption-line spectra of 29 early-type host galaxies of local SNe Ia and found a higher specific SN rate in E–S0 galaxies with ages below 3 Gyr than in older hosts. Recall that the rate of Type Ia SNe can be represented as a linear combination of 'prompt' and 'delayed' (tardy) components (e.g. Scannapieco & Bildsten 2005). The prompt component is more closely related with the recent SFR, and the delayed component with the total stellar mass of galaxy (e.g. Mannucci et al. 2005; Hakobyan et al. 2011; Li et al. 2011b). Therefore, according to Gallagher et al. (2008), the higher rate seen in the youngest E–S0 hosts may be a result of recent star formation and represents a tail of the prompt SN Ia progenitors.

Most recently, Panther et al. (2019) analysed the explosion sites of 11 spectroscopically identified nearby 91bg-like SNe in hosts with different morphologies (including only six E–S0 galaxies) and found that the majority of the stellar populations that host these events are dominated by old stars with lack of recent

[1]The subclasses of Type Ia SNe, discovered in lenticular and spiral host galaxies, will be the subject of a forthcoming paper in this series.

star formation evidence. These authors concluded that the 91bg-like SN progenitors are likely to have delay times, i.e. the time intervals between the SN Ia progenitor formation and the subsequent thermonuclear explosion, much longer (>6 Gyr, see also Crocker et al. 2017) than the typical delay times of normal SNe Ia in star-forming environments, whose delay times peak between several hundred Myr and ∼1 Gyr (e.g. Childress, Wolf & Zahid 2014; Maoz, Mannucci & Nelemans 2014).

The goal of this paper is to properly address these questions through a comparative study of the galactocentric distributions of normal and 91bg-like SNe, as well as through an analysis of the global properties of SNe Ia hosts (e.g. stellar mass, metallicity, colour, and age of stellar population) in a well-defined and morphologically non-disturbed sample of more than 100 relatively nearby elliptical galaxies.

This is the sixth paper of the series following Hakobyan et al. (2012), Hakobyan et al. (2014), Hakobyan et al. (2016), Aramyan et al. (2016), and Hakobyan et al. (2017) and the content is as follows. The sample selection and reduction are presented in Section 2. All the results are presented in Section 3. Section 4 discusses the results with comprehensive interpretations, and summarizes our conclusions. To conform to values used in the series of our articles, Hubble constant $H_0 = 73\,\mathrm{km\,s^{-1}\,Mpc^{-1}}$ is adopted in this paper.

2 SAMPLE SELECTION AND REDUCTION

We used the updated versions of the Asiago Supernovae Catalogue[2] (ASC; Barbon et al. 1999) and Open Supernova Catalog (OSC; Guillochon et al. 2017) to include all spectroscopically classified Type Ia SNe with distances ≤ 200 Mpc ($0.003 \leq z \leq 0.046$),[3] discovered before 2018 October 9. All SNe are required to have equatorial coordinates and/or offsets (positions in arcsec) with respect to host galactic nuclei. We cross-matched these coordinates with the coverage of the SDSS Data Release Fifteen (DR15; Aguado et al. 2019) to identify the host galaxies with elliptical morphology, using the techniques presented in Hakobyan et al. (2012). Many of the identified SNe Ia host galaxies are already listed in data base of Hakobyan et al. (2012), which is based on the SDSS DR8. However, because we added new SNe Ia, for homogeneity we redid the whole reduction for the sample of elliptical host galaxies of this study based only on DR15.

Following the approach of Hakobyan et al. (2014), we checked also the levels of morphological disturbances of the host galaxies using the SDSS images. Because we are interested in studying the distribution of SNe Ia in non-disturbed elliptical galaxies, the hosts with interacting, merging, and post-merging/remnant attributes are removed from the sample.

For three SNe (1980I, 2008gy, and 2018ctv), the almost equality of projected distances from the few nearest elliptical galaxies did not allow to unambiguously assign them to certain hosts. Therefore, we simply excluded these objects from our sample.

For the remaining SNe Ia that satisfy the above mentioned criteria, we carried out an extensive literature search to collect their spectroscopic subclasses (e.g. normal, 91T-like, 91bg-like, and other peculiar events), which are available at the moment of writing this paper. To accomplish this, we mainly used the Weizmann Interactive Supernova data REPository (WISeREP; Yaron & Gal-Yam 2012), which is an interactive archive of SN spectra and photometry, including data of historical events and ongoing surveys/programs. The archive provides also the important references to the original publications, which we considered along with the Astronomer's Telegram[4] (ATEL), website of the Central Bureau for Astronomical Telegrams[5] (CBAT) and other supporting publications (e.g. Branch et al. 1993; Silverman et al. 2012; Tomasella et al. 2014). In total, we managed to collect the subclasses for 109 SNe in 104 host galaxies: 66 SNe are normal, 41 SNe are 91bg-like, and two SNe are 06gz-like (super-Chandrasekhar) events. As expected (e.g. Howell 2001; Gallagher et al. 2005), 91T-like events have not been discovered in elliptical galaxies. On the other hand, less than a dozen of 06gz-like SNe have been discovered so far, and they have a tendency to explode in low-mass (low-metallicity) late-type galaxies (e.g. Taubenberger et al. 2011). Therefore, they are not the subject of our study, and because of only two such objects in our sample, further in the article we do not specifically discuss these events and their hosts, instead we just present them for illustrative purpose.

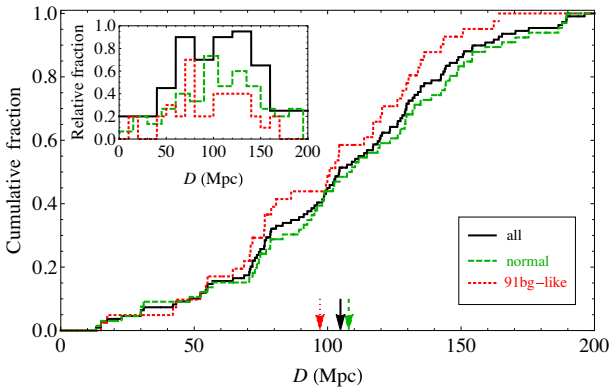

Figure 1. Cumulative and relative (inset) fractions of 109 Type Ia SNe (all – black solid, normal – green dashed, and 91bg-like – red dotted) in elliptical galaxies as a function of distance. The mean values of the distributions are shown by arrows.

It is important to note that in this sample of SNe Ia only seven normal events (∼6 per cent of objects: 1939A, 1957B, 1970J, 1981G, 1982W, 1993ae, and 1993C) were discovered photographically, while all the other 102 SNe were discovered by visual or mostly CCD searches.

Fig. 1 shows the distributions of relative and cumulative fractions of the subclasses of Type Ia SNe as a function of distances. As was mentioned, the 91bg-like SNe have peak luminosities that are ∼2 mag lower than normal SNe Ia (see Taubenberger et al. 2008, and references therein), therefore the discoveries of 91bg-like events might be complicated at greater distances. The mean distances of all, normal, and 91bg-like SNe are 105, 108, and 97 Mpc with standard deviations of 43, 44, and 38 Mpc, respectively. Meanwhile, the two-sample Kolmogorov–Smirnov (KS) and Anderson–Darling (AD) tests[6] showed that the distance distributions of normal and 91bg-like events are not significantly different ($P_{KS} = 0.404$, $P_{AD} = 0.238$) and could thus be drawn from the same parent distribution. Therefore,

[2]The ASC was terminated as at 2017 December 31.

[3]Following Hakobyan et al. (2012), to calculate the luminosity distances of SNe/host galaxies, we used the recession velocities both corrected to the centroid of the Local Group (Yahil, Tammann & Sandage 1977), and for infall of the Local Group towards Virgo cluster (Theureau et al. 1998; Terry, Paturel & Ekholm 2002).

[4]See http://www.astronomerstelegram.org/.

[5]See http://www.cbat.eps.harvard.edu/iau/cbat.html.

[6]Traditionally, we adopted in this article the threshold of 5 per cent for significance levels (P-values) of the different tests. For more details of the statistical tests, the reader is referred to Engmann & Cousineau (2011).

our subsamples of normal and 91bg-like SNe and their host galaxies should not be strongly affected by the redshift-dependent biases against or in favour of one of the SN subclasses.

We measured the photometry and geometry of the 104 host galaxies according to the approaches presented in Hakobyan et al. (2012). For each host galaxy, we used the fitted 25 mag arcsec^{-2} elliptical aperture in the SDSS g-band to obtain the major axis (D_{25}), elongation (a/b), and position angle (PA) of the major axis relative to North in the anticlockwise direction. The classification of hosts includes also the ratio $10(a-b)/a$: for a projection of a galaxy with a equal to b, the ratio is 0 and the morphological type is E0. There are only one E5 and 10 E4 host galaxies (∼10 per cent of the sample). The rest of the galaxies are almost evenly distributed in E0–E3 bins. The mean D_{25} of the hosts is 129 arcsec with the minimum value of 21 arcsec. The corresponding u-, g-, r-, i-, and z-band fluxes (apparent magnitudes)[7] are measured using the g-band fitted elliptical aperture. During the measurements, we masked out bright projected and/or saturated stars. The apparent/absolute magnitudes and D_{25} values are corrected for Galactic extinction using the Schlafly & Finkbeiner (2011) recalibration of the Schlegel, Finkbeiner & Davis (1998) infrared-based dust map. These values are not corrected for host galaxy internal extinction because ellipticals have almost no global extinction, with mean $A_V = 0.01 \pm 0.01$ mag (González Delgado et al. 2015). Since the redshifts of host galaxies are low ($z \leq 0.046$), the accounted K-corrections for the magnitudes are mostly negligible and do not exceed 0.2 mag in the g-band. The D_{25} values are also corrected for inclination/elongation effect according to Bottinelli et al. (1995).

In an elliptical galaxy the real galactocentric distance of SN cannot be calculated using the SN offset from the host galaxy nucleus ($\Delta\alpha$ and $\Delta\delta$). Instead, we can only calculate the projected galactocentric distance of an SN ($R_{\rm SN} = \sqrt{\Delta\alpha^2 + \Delta\delta^2}$), which is the lower limit of the real galactocentric distance.[8] Following Ivanov et al. (2000), we used the relative projected galactocentric distances ($\widetilde{R}_{\rm SN} = R_{\rm SN}/R_{25}$), i.e. normalized to $R_{25} = D_{25}/2$ in the g-band.

However, for the normalization, the effective radius ($R_{\rm e}$) could be more relevant being tighter correlated with the stellar surface density distribution or surface brightness profile of the host galaxy in comparison with the R_{25} photometric radius (e.g. Kormendy et al. 2009). For elliptical galaxies, the surface brightness (I) profiles are described by the Sérsic law (Sérsic 1963)

$$I(R\,|\,R_{\rm e}) = I_0 \exp\left\{-b_{\rm n}\left(\frac{R}{R_{\rm e}}\right)^{\frac{1}{n}}\right\}, \qquad (1)$$

where $R_{\rm e}$ is the radius of a circle that contains half of the light of the total galaxy (also known as half-light radius), I_0 is the central surface brightness of the galaxy, n is the Sérsic index, defining the shape of the profile. An analytical expression that approximates the $b_{\rm n}$ parameter is $b_{\rm n} \simeq 1.9992\,n - 0.3271$ (e.g. Capaccioli 1989). When $n = 4$, the profile, which is called de Vaucouleurs profile, sufficiently describes the surface brightness distribution of elliptical galaxies (de Vaucouleurs 1948). Therefore, following Förster & Schawinski (2008), we also normalized $R_{\rm SN}$ to the $R_{\rm e}$ radii of host galaxies ($\widehat{R}_{\rm SN} = R_{\rm SN}/R_{\rm e}$).

[7]All magnitudes are in the AB system such that $u_{\rm AB} = u - 0.04$ mag and $z_{\rm AB} = z + 0.02$ mag (g, r, and i are closer to AB system, see https://www.sdss.org/dr15/algorithms/fluxcal/).

[8]In several cases when SNe offsets were not available in the above mentioned catalogues, we calculated $\Delta\alpha$ and $\Delta\delta$ by $\Delta\alpha \approx (\alpha_{\rm SN} - \alpha_{\rm g})\cos\delta_{\rm g}$ and $\Delta\delta \approx (\delta_{\rm SN} - \delta_{\rm g})$, where $\alpha_{\rm SN}$ and $\delta_{\rm SN}$ are SN coordinates and $\alpha_{\rm g}$ and $\delta_{\rm g}$ are host galaxy coordinates in equatorial system.

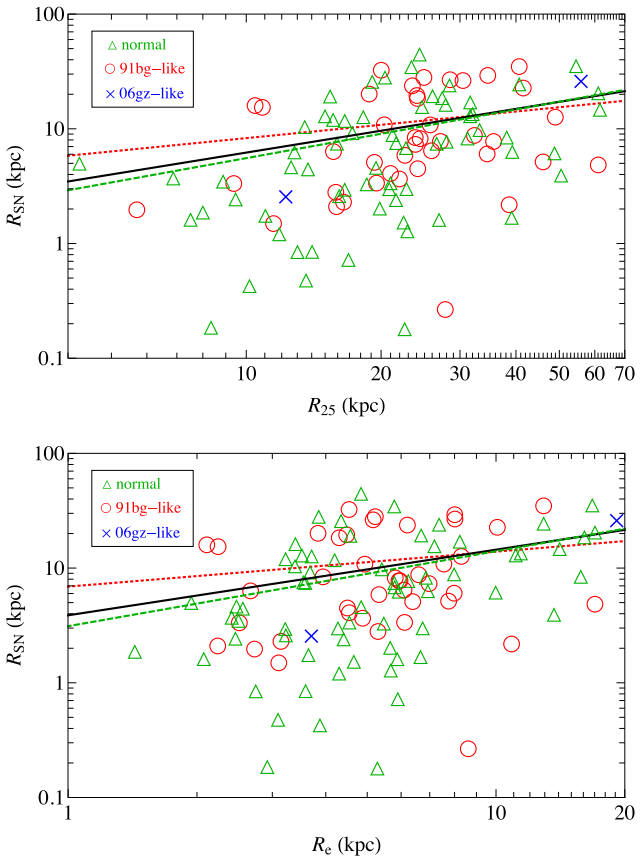

Figure 2. Upper panel: comparison of the projected galactocentric distances of SNe Ia and R_{25} of elliptical host galaxies in kpc. Green triangles, red circles, and blue crosses show normal, 91bg-like, and 06gz-like SNe, respectively. Black solid (all), green dashed (normal), and red dotted (91bg-like) lines are best fits to the samples. Bottom panel: same as in upper panel but for $R_{\rm SN}$ versus $R_{\rm e}$.

The g-band $R_{\rm e}$ radii (in arcsec) of our host galaxies are extracted from the SDSS where a detailed photometric analysis of galaxies is performed (Lupton et al. 2001). Their pipeline fitted galaxies with a de Vaucouleurs profile and an exponential profile,[9] and asked for the linear combination of the two that best fitted the image, providing the $R_{\rm e}$ and parameter fracDeV, which is the fraction of fluxes contributed from the de Vaucouleurs profile. An elliptical galaxy with a pure de Vaucouleurs profile should have fracDeV = 1, and a galaxy with pure exponential profile should have fracDeV = 0. In our morphologically selected sample of hosts, most (about 90 per cent) of the galaxies have fracDeV > 0.8, where fracDeV = 0.8 roughly corresponds to S0 galaxies (e.g. Bernardi et al. 2006). Only for 14 host galaxies (mostly with $D_{25} > 200$ arcsec), the SDSS lacks the mentioned model fits or provides unreliable parameters due to the blending/defragmenting of galaxies with large angular sizes. For these 14 galaxies, we used our estimations of half-light radii based on the SDSS g-band images.

The R_{25} and $R_{\rm e}$ normalizations are crucial for studying the projected radial distribution of SNe, because the distribution of linear values of $R_{\rm SN}$ is strongly biased by the greatly different intrinsic sizes of elliptical hosts. Fig. 2 illustrates the dependencies

[9]The Sérsic index of $n = 1$ represents the exponential profile of S0–Sm galactic discs (Freeman 1970).

Table 1. The best fits from Fig. 2 with results of the Spearman's rank correlation test.

SN subclass	N_{SN}	a	b	r_s	P
		$\log(R_{SN}[\text{kpc}]) = a + b\ \log(R_{25}[\text{kpc}])$			
all	109	0.16 ± 0.25	0.63 ± 0.17	0.457	$\mathbf{6 \times 10^{-7}}$
normal	66	0.04 ± 0.32	0.70 ± 0.22	0.481	$\mathbf{4 \times 10^{-5}}$
91bg-like	41	0.53 ± 0.44	0.39 ± 0.30	0.316	**0.044**
		$\log(R_{SN}[\text{kpc}]) = a + b\ \log(R_e[\text{kpc}])$			
all	109	0.59 ± 0.13	0.57 ± 0.14	0.364	$\mathbf{10^{-4}}$
normal	66	0.49 ± 0.17	0.65 ± 0.19	0.414	$\mathbf{5 \times 10^{-4}}$
91bg-like	41	0.84 ± 0.23	0.30 ± 0.28	0.162	0.313

Note. Spearman's coefficient r_s is a non-parametric measure of rank correlation ($r_s \in [-1; 1]$), it assesses how well the relationship between two variables can be described using a monotonic function. The statistically significant correlations (P-values ≤ 0.05) are highlighted in bold.

of the R_{SN} on R_{25} and R_{SN} on R_e of host galaxies in kpc. The best fits from Fig. 2 and results of the Spearman's rank correlation test for R_{SN} versus R_{25} and for R_{SN} versus R_e (regardless of log or linear scales) are presented in Table 1. The Spearman's rank test indicates significant positive trends ($r_s > 0$) between the R_{SN} and R_{25} for all, normal, and 91bg-like SNe, as well as between the R_{SN} and R_e for all and normal SNe Ia. Only for 91bg-like SNe in the latter case, the trend is positive again but not statistically significant. In the remainder of this study, we use only normalized projected galactocentric radii of Type Ia SNe, i.e. $\widetilde{R}_{SN} = R_{SN}/R_{25}$ and $\widehat{R}_{SN} = R_{SN}/R_e$.

In addition, we measured the integrated g-band flux of the concentric elliptical aperture, which crosses the position of an SN, with the same elongation and PA as the host galaxy aperture. We then normalized this flux to the total flux contained within an elliptical aperture, retaining the same elongation and PA, out to distances where the host galaxy flux is consistent with the sky background values. This fractional radial g-band flux is commonly referred as Fr_g and can have values between 0 and 1, where a value of 0 means that an SN explodes at the centre of its host, while a value of 1 means that the SN explodes at distances where no significant galaxy flux is detected, i.e. at the edge of the galaxy. As will be presented in Section 3.3, the distribution of Fr_g values allows to compare the radial distribution of SNe Ia with respect to that of the g-band light of host galaxies, irrespective of their different elongations and Sérsic indices (elliptical galaxies can have $n \approx 2$–6 in the g-band, see e.g. Nair & Abraham 2010; Vika et al. 2013). Note that 15 SNe, which are located far outside the elliptical apertures where fluxes are consistent with the sky background values, are removed from the Fr_g analysis in Section 3.3.[10] For a complete description of the adopted methodology of Fr_g measurement, the reader is referred to James & Anderson (2006) and Anderson & James (2009).

The full data base of 109 individual SNe Ia (SN designation, subclass, source of the subclass, offset from host galaxy nucleus, and fractional radial g-band flux) and their 104 elliptical hosts (galaxy SDSS designation, distance, a/b, PA, R_e, corrected D_{25} and u-, g-, r-, i-, z-band absolute magnitudes) is available in the online version (Supporting Information) of this article.

[10]Their inclusion would artificially increase the number of SNe Ia in the fractional radial flux distribution at $Fr_g = 1$ (see Section 3.3).

Table 2. Comparison of the projected and normalized distributions of the subclasses of Type Ia SNe along major (U) and minor (V) axes of elliptical host galaxies.

SN subclass	N_{SN}	Subsample 1	versus	Subsample 2	P_{KS}	P_{AD}
		$\langle\lvert U\rvert/R_{25}\rangle$		$\langle\lvert V\rvert/R_{25}\rangle$		
all	109	0.31 ± 0.03	versus	0.26 ± 0.03	0.141	0.052
normal	66	0.27 ± 0.03	versus	0.27 ± 0.05	0.438	0.250
91bg-like	41	0.37 ± 0.06	versus	0.26 ± 0.05	0.279	0.143
		$\langle\lvert U\rvert/R_e\rangle$		$\langle\lvert V\rvert/R_e\rangle$		
all	109	1.31 ± 0.13	versus	1.13 ± 0.15	0.331	0.099
normal	66	1.09 ± 0.14	versus	1.10 ± 0.21	0.721	0.352
91bg-like	41	1.68 ± 0.27	versus	1.21 ± 0.23	0.420	0.210

Note. The P_{KS} and P_{AD} are the probabilities from two-sample KS and AD tests, respectively, that the two distributions being compared (with respective mean values) are drawn from the same parent distribution. To calculate the P_{KS} and P_{AD}, we used the calibrations by Massey (1951) and Pettitt (1976), respectively.

3 RESULTS

With the aim of finding possible links between the properties of SN progenitors and host stellar populations of elliptical galaxies, we now study the distributions of projected and normalized galactocentric distances and fractional radial fluxes of the subclasses of Type Ia SNe (normal and 91bg-like events). In this section, we also study the possible differences of global properties (absolute magnitudes, colour, R_{25}, and R_e) and estimates of the physical parameters (stellar mass, metallicity, and age) of the stellar population of elliptical galaxies in which the different subclasses of SNe Ia are discovered.

3.1 Directional (major versus minor axes) distributions of SNe Ia in elliptical host galaxies

Because the elliptical host galaxies of Type Ia SNe have different elongations (noted in Section 2), it is possible that the distributions of projected galactocentric distances of SNe along major (U) and minor (V) axes, normalized to R_{25} or R_e, would be different. Obviously, the projected U and V galactocentric distances (in arcsec) of an SN are

$$U = \Delta\alpha\ \sin\text{PA} + \Delta\delta\ \cos\text{PA}\,,$$
$$V = \Delta\alpha\ \cos\text{PA} - \Delta\delta\ \sin\text{PA}\,.$$

Here, as already noted, $\Delta\alpha$ and $\Delta\delta$ are offsets of the SN in equatorial system, and PA is position angle of the major axis of the elliptical host galaxy.

In the mentioned context, using the two-sample KS and AD tests, we compare the distributions of $|U|/R_{25}$ versus $|V|/R_{25}$, as well as the distributions of $|U|/R_e$ versus $|V|/R_e$ for all, normal, and 91bg-like SNe. Here, the absolute values of U and V are used to increase the statistical power of the tests. The values of P_{KS} and P_{AD} in Table 2 show that the distributions of projected and normalized galactocentric distances of SNe along major and minor axes are consistent between each other. Only the P_{AD} values for the entire sample of SNe Ia are close to the rejection threshold of 0.05, however when we split the sample between normal and 91bg-like events, both the P-values of KS and AD tests become clearly above the threshold. Therefore, the different elongations of elliptical host galaxies in our sample have negligible impact, if any, on the sky plane projection of the spherical 3D distribution of SNe Ia.

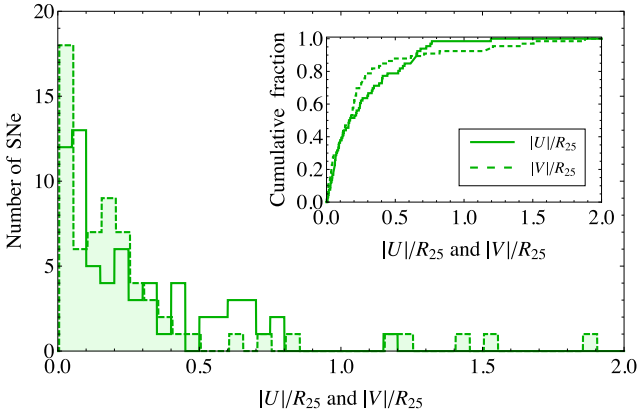

Figure 3. Distributions of $|U|/R_{25}$ (green solid) and $|V|/R_{25}$ (green dashed and filled) values for normal SNe Ia. The inset presents the corresponding cumulative distributions.

For illustration, in Fig. 3 we show the histograms and cumulative distributions of $|U|/R_{25}$ and $|V|/R_{25}$ for normal SNe Ia. Comparison of the same distributions for 91bg-like SNe looks similar (also for the cases with R_e normalization). Fig. 4 shows the projected distributions of the subclasses of Type Ia SNe with R_{25} and R_e normalizations.

3.2 The radial distributions of SNe Ia in ellipticals

As already mentioned above, the light profiles of elliptical galaxies are characterized with a continuous distribution according to the Sérsic law with mean index $n \approx 4$, when considering the families of ellipticals from dwarfs to giants (for the g-band see e.g. Nair & Abraham 2010; Vika et al. 2013). In addition, Förster & Schawinski (2008) have already shown that the projected surface density distribution of Type Ia SNe in morphologically selected early-type host galaxies is consistent with the de Vaucouleurs profile ($n = 4$) in the $0.2 < R_{SN}/R_e < 4$ radial range (see also Tsvetkov et al. 2004; Dilday et al. 2010). However, in the literature a comprehensive analysis of the surface density distributions of normal and 91bg-like SNe in well-defined elliptical host galaxies with different radius normalizations has not yet been performed and, as already mentioned, is one of the main goals of this study.

Using maximum likelihood estimation (MLE) method, we fit the distribution of projected and R_{25}-normalized galactocentric radii of Type Ia SNe ($\widetilde{R}_{SN} = R_{SN}/R_{25}$) with the surface density model of Sérsic profile with $n = 4$. If the surface density (Σ) of SNe Ia is described by a Sérsic function of $\widetilde{R}_{SN}$ (see equation 1), then the probability that an SN is observed at $\widetilde{R}_{SN}$ radius, i.e. probability density function (PDF), is

$$p(\widetilde{R}_{SN}|\widetilde{R}_e^{SN}) = \frac{\widetilde{R}_{SN}\,\Sigma(\widetilde{R}_{SN}|\widetilde{R}_e^{SN})}{\int_0^\infty \widetilde{R}_{SN}\,\Sigma(\widetilde{R}_{SN}|\widetilde{R}_e^{SN})\,\mathrm{d}\widetilde{R}_{SN}}\,, \tag{2}$$

where $\widetilde{R}_e^{SN} = R_e^{SN}/R_{25}$ is normalized effective radius of SN distribution. The likelihood of the set of $\{\widetilde{R}_{SN\,i}\}$ is

$$\mathcal{L}(\widetilde{R}_e^{SN}) = \prod_{i=1}^{N_{SN}} p(\widetilde{R}_{SN\,i}|\widetilde{R}_e^{SN})\,, \tag{3}$$

and thus maximizing $\ln(\mathcal{L})$ we get the effective radii of SN distributions for the subclasses of Type Ia SNe.

At the same time, to check whether the distributions of SNe Ia follow the best-fitting de Vaucouleurs profiles, we perform one-sample KS and AD tests on the cumulative distributions of the projected and normalized galactocentric distances of SNe. In general, the cumulative distribution function (CDF) of Sérsic model can be expressed as the integral of its PDF (see equation 2) as follows:

$$E(\widetilde{R}_{SN}) = \int_{-\infty}^{\widetilde{R}_{SN}} p(t\,|\widetilde{R}_e^{SN})\,\mathrm{d}t$$
$$= 1 - \Gamma\left(2n,\ b_n\left(\frac{\widetilde{R}_{SN}}{\widetilde{R}_e^{SN}}\right)^{\frac{1}{n}}\right)\Big/\Gamma\left(2n\right), \tag{4}$$

where

$$\Gamma(z) = \int_0^\infty t^{z-1}\mathrm{e}^{-t}\mathrm{d}t$$

and

$$\Gamma(a,\ z) = \int_z^\infty t^{a-1}\mathrm{e}^{-t}\mathrm{d}t$$

are the complete and upper incomplete gamma functions, respectively.

For the R_e normalization, in the above mentioned formulae (equations 2–4) we simply replace $\widetilde{R}_{SN}$ with $\widehat{R}_{SN} = R_{SN}/R_e$ and therefore $\widetilde{R}_e^{SN}$ with $\widehat{R}_e^{SN} = R_e^{SN}/R_e$. The estimated $\widetilde{R}_e^{SN}$ and $\widehat{R}_e^{SN}$ effective radii, and the P_{KS} and P_{AD} probabilities that the distributions of SNe Ia are drawn from the best-fitting de Vaucouleurs surface density profiles (Sérsic model with $n = 4$) are listed in Table 3.

From the P-values in Table 3, we see that the global ($\widetilde{R}_{SN} \geq 0$ and $\widehat{R}_{SN} \geq 0$) surface density distributions of Type Ia SNe in elliptical host galaxies are not consistent with the de Vaucouleurs profiles. When splitting the sample between the subclasses of SNe Ia, we see that the significant inconsistency exists for the $\widetilde{R}_{SN}$ distribution of 91bg-like events, and the marginal inconsistency takes place for the $\widehat{R}_{SN}$ distribution of the same SNe (Table 3). The left-hand panel of Fig. 5 illustrates that the main inconsistency is likely attributed to the slower growth or decline (in case of 91bg-like events) of the SN surface density at the central region of hosts with the radius of about one tenth of the optical radius of galaxies (grey shaded region in the figure). In our sample, the mean R_e/R_{25} is about four, and a similar behaviour of the R_e-normalized surface density is seen at the central $0.4R_e$ region (grey shaded region in the right-hand panel of Fig. 5).

It is important to note that different SN surveys are biased against the discovery of SNe near the centres of host galaxies (e.g. Leaman et al. 2011). This happens because central SNe have lower contrast with respect to the bright and often overexposed background of elliptical hosts, increasing the difficulty of their detection in a scan of the survey figures (e.g. Hamuy & Pinto 1999). In addition, host galaxy internal extinction $A_V < 0.2$ mag exists only within the central region, while A_V is almost zero outside that region till to the end of optical radius of an elliptical galaxy (González Delgado et al. 2015). Since 91bg-like events have peak luminosities that are ∼2 mag lower than normal SNe Ia (e.g. Taubenberger et al. 2008 and references therein), 91bg-like SNe are more strongly affected by these effects than are normal Type Ia SNe (as seen in Fig. 5).

We now exclude SNe from the central regions of hosts ($\widetilde{R}_{SN} \geq 0.1$, $\widehat{R}_{SN} \geq 0.4$) and compare the SN distributions with the best-fitting inner-truncated de Vaucouleurs profiles. From the P-values in Table 3, we see that all the inconsistencies vanish. In Fig. 5, we show the inner-truncated de Vaucouleurs profiles, extended to

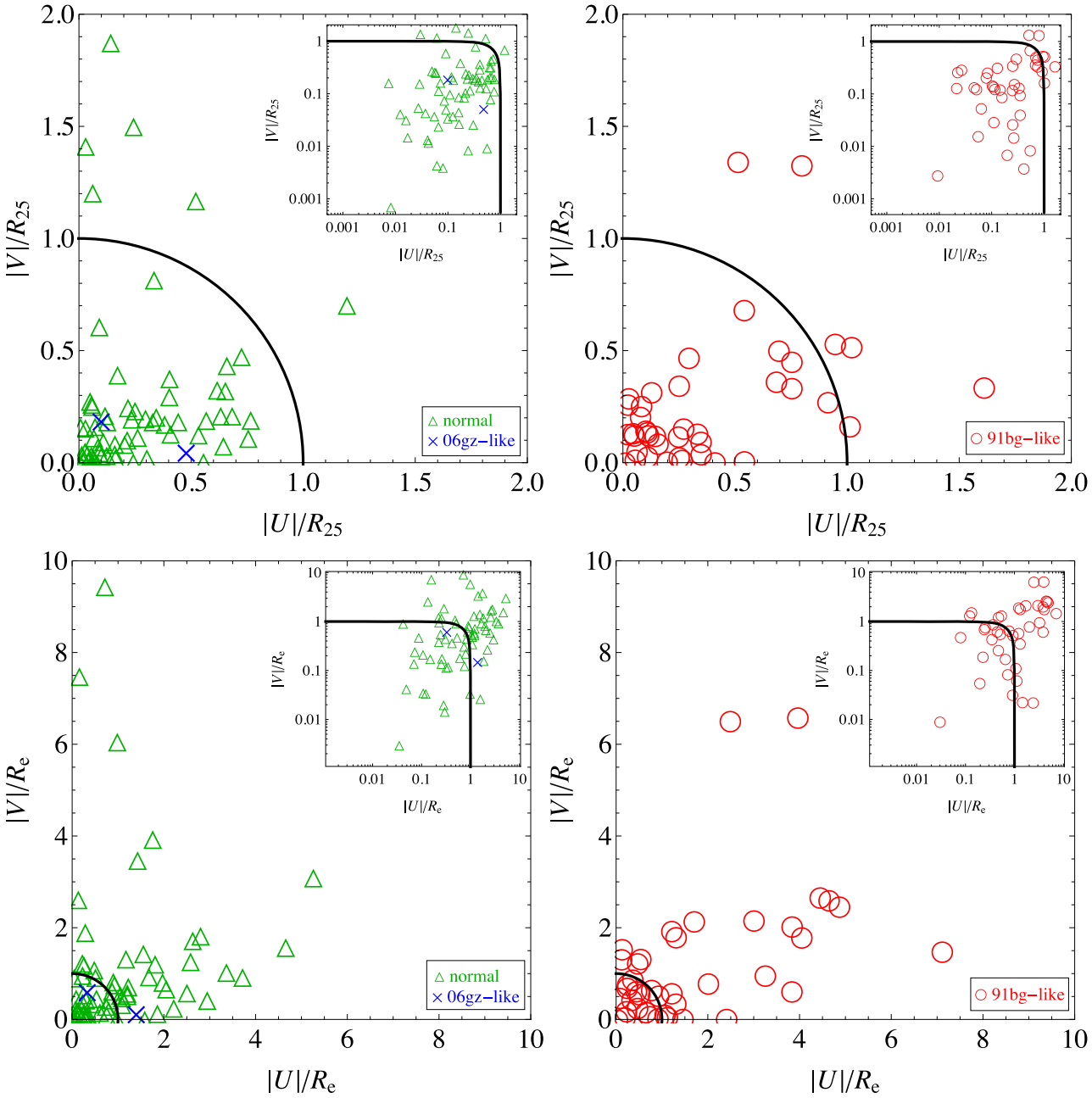

Figure 4. Upper panels: projected and R_{25}-normalized distributions of the different subclasses of Type Ia SNe along major (U) and minor (V) axes of elliptical host galaxies. The green triangles, blue crosses, and red circles represent normal, 06gz-like, and 91bg-like SNe, respectively. The quarters of big black circles are the host galaxy R_{25} sizes. Bottom panels: same as in upper panels but for R_e normalization. The quarter circles now represent R_e. In the insets, we show the same distributions with log axes.

the central regions of host galaxies,[11] and the global surface density distributions of SNe, enabling to roughly estimate the loss in SNe Ia discoveries, most expressive for 91bg-like events, compared with their expected densities. The mean loss of SNe in the central regions of elliptical galaxies is 22 ± 4 per cent of the expected total number of Type Ia SNe. This value is in good agreement with the similar estimation of 23 ± 12 per cent in E–S0 galaxies by Cappellaro & Turatto (1997), though a different method and sample were used in their study. In our sample, the mean central losses of normal and 91bg-like SNe are 17 ± 5 and 27 ± 7 per cent, respectively.

In addition, we check the dependence of the described bias, i.e. the central loss of SNe, on the distances of their host galaxies (the *Shaw effect*; Shaw 1979), splitting the sample between near ($\leq$100 Mpc) and far (>100 Mpc) objects. This separation is done to have adequate numbers of objects in the subsamples. The

[11] For illustrative purpose, in the left-hand panel of Fig. 5 we also present the best-fitting inner-truncated exponential profile (black thin line, i.e. $n = 1$ in equation 1). The one-sample KS and AD tests show that the surface density distribution of SNe Ia is strongly inconsistent with the global ($P_{KS} = 0.050$, $P_{AD} = 0.005$) and inner-truncated ($P_{KS} = 0.090$ [barely inconsistency], $P_{AD} = 0.039$) exponential models.

Table 3. Consistency of the distribution of projected and normalized galactocentric distances of SNe Ia with the surface density model of Sérsic profile with $n = 4$ (de Vaucouleurs profile) in elliptical host galaxies.

SN subclass	$\widetilde{R}_{\rm SN} \geq$	$N_{\rm SN}$	$\widetilde{R}_{\rm e}^{\rm SN}$	$P_{\rm KS}$	$P_{\rm AD}$
all	0	109	0.28 ± 0.03	**0.008**	**0.014**
normal	0	66	0.26 ± 0.04	0.184	0.129
91bg-like	0	41	0.31 ± 0.04	**0.036**	**0.041**
all	0.1	94	0.18 ± 0.02	0.231	0.093
normal	0.1	54	0.18 ± 0.02	0.369	0.222
91bg-like	0.1	38	0.18 ± 0.04	0.263	0.185
	$\widehat{R}_{\rm SN} \geq$		$\widehat{R}_{\rm e}^{\rm SN}$		
all	0	109	1.15 ± 0.12	**0.016**	**0.034**
normal	0	66	1.03 ± 0.09	0.176	0.212
91bg-like	0	41	1.38 ± 0.15	0.059	0.068
all	0.4	92	0.80 ± 0.12	0.132	0.093
normal	0.4	52	0.78 ± 0.18	0.144	0.196
91bg-like	0.4	38	0.87 ± 0.21	0.514	0.206

Note. The $P_{\rm KS}$ and $P_{\rm AD}$ are the probabilities from one-sample KS and AD tests, respectively, that the distributions of SNe Ia are drawn from the best-fitting de Vaucouleurs surface density profiles with the maximum likelihood values of $\widetilde{R}_{\rm e}^{\rm SN} = R_{\rm e}^{\rm SN}/R_{25}$ and $\widehat{R}_{\rm e}^{\rm SN} = R_{\rm e}^{\rm SN}/R_{\rm e}$ (with bootstrapped errors, repeated 10^3 times). The $P_{\rm KS}$ and $P_{\rm AD}$ are calculated using the calibrations by Massey (1951) and D'Agostino & Stephens (1986), respectively. The statistically significant deviations from de Vaucouleurs profile (P-values $\leq$ 0.05) are highlighted in bold.

surface density distributions of SNe in these distance bins show the equivalent central losses of SNe. In this sense, it is well known that the Shaw effect is important for photographic searches and negligible for visual/CCD searches (e.g. Howell, Wang & Wheeler 2000). Similarly, the Shaw effect is negligible in our sample, in which ∼94 per cent of SNe Ia are discovered via visual and CCD searches (see Section 2).

3.3 SNe Ia locations versus fractional radial light distributions of elliptical hosts

In the analysis above, we fixed the Sérsic index to $n = 4$ in equation (1) when describing the surface density distribution of SNe Ia, while different elliptical host galaxies have $n \approx 2$–6 in the SDSS g- band (e.g. Nair & Abraham 2010; Vika et al. 2013). Fortunately, the distribution of fractional radial g-band fluxes of SNe (Fr_g, see Section 2 for definition) allows to compare the distribution of SNe with respect to that of the g-band light of elliptical host galaxies, irrespective of their different Sérsic indices and elongations (e.g. Förster & Schawinski 2008). If the SNe Ia are equally likely to arise from any part of the projected light distribution of the host galaxies, i.e. the surface brightness of galaxy I and the surface density of SNe Σ are related by $\Sigma = {\rm Const} \times I$, then one would expect that the Fr_g values are evenly distributed throughout the projected radii of hosts (a flat distribution, independent of radius) and the $\langle Fr_g \rangle = 0.5$ (e.g. James & Anderson 2006). For the Fr_g values (from 0 to 1), the PDF and CDF are

$$p(Fr_g) = 1 \quad \text{and} \quad E(Fr_g) = Fr_g\,, \tag{5}$$

respectively.

From the P-values of one-sample KS and AD tests in Table 4, we see that the Fr_g distribution of Type Ia SNe is not consistent with the g-band light distribution of elliptical host galaxies (for the KS statistic but marginally so in the AD statistic), mainly due to the distribution of 91bg-like events. The upper panel of Fig. 6 illustrates that, as already stated above, the main inconsistency is due to the

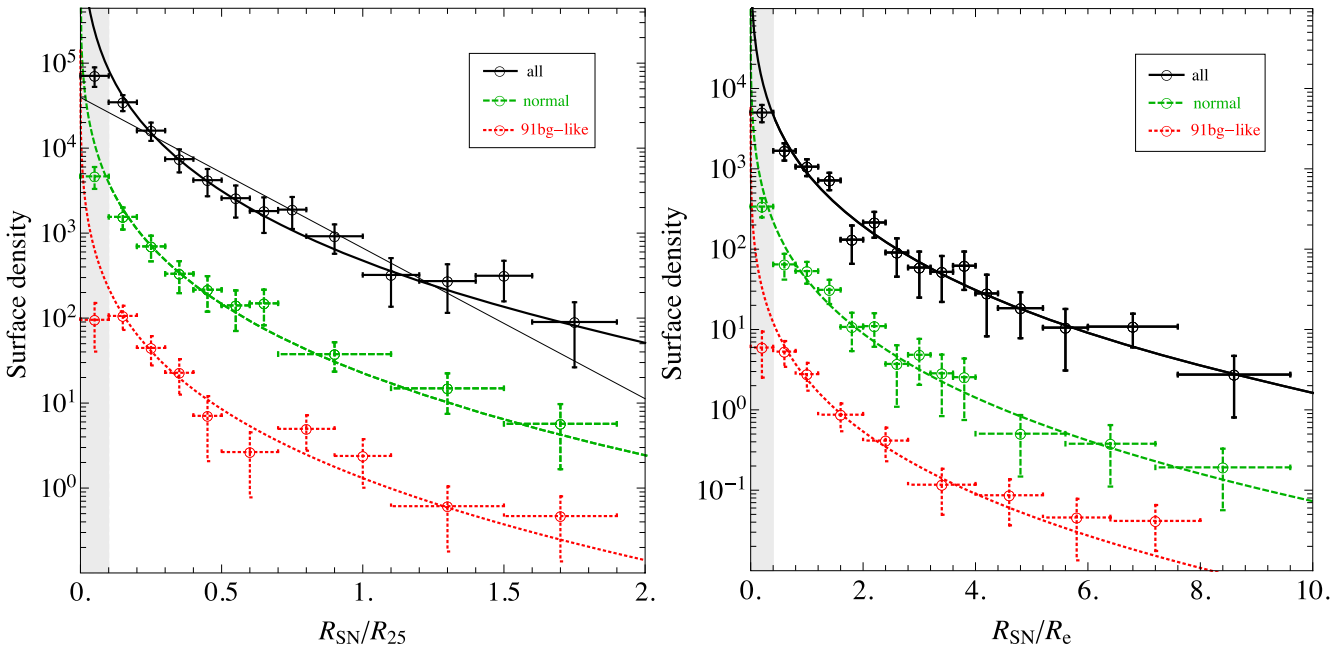

Figure 5. Left: R_{25}-normalized surface density distributions (arbitrary scaled) of all (black solid), normal (green dashed), and 91bg-like (red dotted) SNe Ia in elliptical host galaxies. The vertical error bars assume a Poisson distribution. The horizontal bars show the bin sizes that are increased at the edges of galaxies to include at least two SNe in each. The different curves show the maximum likelihood de Vaucouleurs surface density profiles, estimated using the inner-truncated distributions (outside the shaded area). For all SNe, the best-fitting inner-truncated exponential profile (black thin line) is also shown. For better visibility, the distributions with their best-fitting profiles are shifted vertically (to avoid falling one on to another). Right: same as in left-hand panel but for $R_{\rm e}$ normalization.

Table 4. Consistency of the Fr_g (or inner-truncated $\check{F}r_g$) distributions of SNe Ia with the surface brightness distribution of elliptical host galaxies.

SN subclass (Fr_g or $\check{F}r_g$)	N_{SN}	P_{KS}	P_{AD}
all (Fr_g)	94	**0.021**	0.054
normal (Fr_g)	58	0.405	0.436
91bg-like (Fr_g)	34	**0.044**	0.056
all ($\check{F}r_g$)	79	0.482	0.404
normal ($\check{F}r_g$)	46	0.758	0.719
91bg-like ($\check{F}r_g$)	31	0.286	0.257

Note. The P_{KS} and P_{AD} are the probabilities from one-sample KS and AD tests, respectively, that the distributions of Fr_g (or inner-truncated $\check{F}r_g$) are drawn from the surface brightness distribution of host galaxies. The statistically significant deviations (P-values ≤ 0.05) are highlighted in bold. Recall that 15 SNe, which are located far outside the elliptical apertures where fluxes are consistent with the sky background values, are removed from the fractional radial flux analysis (see Section 2).

selection effect against the discovery of SNe Ia near the centre of the host galaxies (also seen in the right-hand panels of fig. 2 in Förster & Schawinski 2008). Therefore, we also use the inner-truncated fractional radial g-band fluxes of SNe ($\check{F}r_g$), excluding the central region of galaxies with one tenth of the optical radius ($0.1\,R_{25}$)

$$\check{F}r_g = \frac{Fr_g - fr_g}{1 - fr_g},$$

where fr_g is the fractional flux of $0.1\,R_{25}$ region. A similar definition of inner-truncated fractional flux for SNe in elliptical galaxies was first used by Maza & van den Bergh (1976).

Simply replacing Fr_g with $\check{F}r_g$ in equations (5) and using one-sample KS and AD tests, we see that the $\check{F}r_g$ distributions of all subclasses of Type Ia SNe are now consistent with the g-band light distribution of hosts, with mean values of $\check{F}r_g$ near 0.5 as predicted (see Table 4 and the bottom panel of Fig. 6).

We now compare, in Table 5, the distributions of $\widetilde{R}_{SN}$, $\widehat{R}_{SN}$, Fr_g, and $\check{F}r_g$ values between the subsamples of normal and 91bg-like SNe, using the two-sample KS and AD tests. The mean values of the distributions are also listed. With the tests, we see no statistically significant differences between the global radial distributions of the SN subclasses. Similar results hold true for the inner-truncated distributions of SNe Ia.

3.4 The global properties of SNe Ia elliptical host galaxies

In the SDSS DR15, different estimates of the parameters of galaxies (e.g. stellar mass, metallicity, and age of stellar population) encompass calculations based on various stellar population models (e.g. Evolutionary Population Synthesis, Maraston 2005; Principal Component Analysis-based model, Chen et al. 2012; Flexible Stellar Population Synthesis, Conroy, Gunn & White 2009), and different assumptions about galaxy extinction and star formation histories.[12] However, from 109 SNe Ia elliptical hosts of our study, only 43 SNe (29 normal, 13 91bg-like, and one 06gz-like) have available SDSS spectra of hosts, thus reliable estimates of mass, age, and metallicity. Therefore, instead of using them we prefer to estimate the stellar masses (M_*) of all our elliptical hosts, using the empirical relation of Taylor et al. (2011) between $\log(M_*/M_\odot)$, $g - i$ colour, and i-band absolute magnitude (M_i) as determined from more than 10^5 galaxies with redshifts $z < 0.65$

$$\log\left(\frac{M_*}{M_\odot}\right) = 1.15 + 0.70(g - i) - 0.4M_i\,, \qquad (6)$$

where M_* has solar mass units. According to Taylor et al., this relation provides an estimate of the stellar mass-to-light ratio (M_*/L_i) to a 1σ accuracy of $\sim$0.1 dex. In addition, to estimate average host galaxy stellar metallicities, we use the Gallazzi et al. (2006) correlation between stellar mass of E–S0 galaxy and $\log(Z_*/Z_\odot)$ as determined from about 26 000 SDSS galaxies (see also Scott et al.

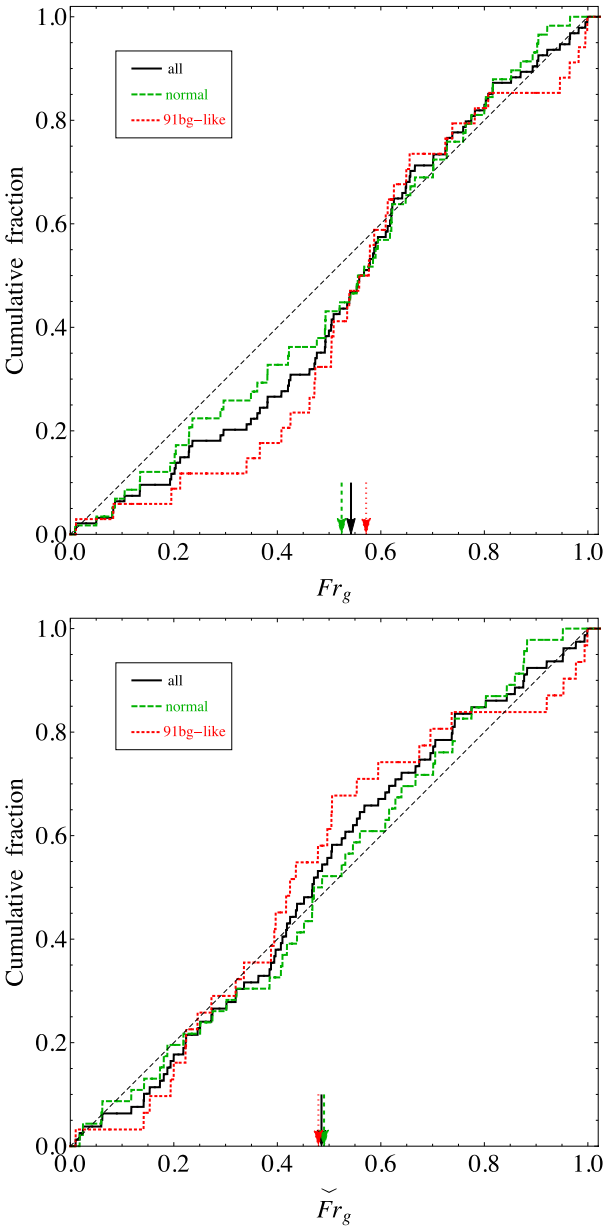

Figure 6. Upper panel: cumulative Fr_g distributions of SNe Ia (all – black solid, normal – green dashed, and 91bg-like – red dotted) with respect to the g-band surface brightness distribution of their elliptical host galaxies (black thin diagonal line). The mean values of the distributions are shown by arrows. Bottom panel: same as in upper panel but for the inner-truncated $\check{F}r_g$ distributions.

[12]For more detailed information with corresponding references, the reader is referred to https://www.sdss.org/dr15/spectro/galaxy/.

Table 5. Comparison of the distributions of $\widetilde{R}_{SN}$, $\widehat{R}_{SN}$, Fr_g, and $\check{F}r_g$ values between the subsamples of normal and 91bg-like SNe.

Parameter	normal		versus	91bg-like		P_{KS}	P_{AD}
	N_{SN}	⟨Parameter⟩		N_{SN}	⟨Parameter⟩		
$\widetilde{R}_{SN} \geq 0$	66	0.43 ± 0.05	versus	41	0.50 ± 0.07	0.456	0.357
$\widetilde{R}_{SN} \geq 0.1$	54	0.52 ± 0.06	versus	38	0.53 ± 0.07	0.700	0.804
$\widehat{R}_{SN} \geq 0$	66	1.77 ± 0.23	versus	41	2.25 ± 0.32	0.502	0.232
$\widehat{R}_{SN} \geq 0.4$	52	2.18 ± 0.26	versus	38	2.41 ± 0.33	0.852	0.820
Fr_g	58	0.52 ± 0.03	versus	34	0.57 ± 0.04	0.606	0.429
$\check{F}r_g$	46	0.49 ± 0.04	versus	31	0.48 ± 0.05	0.677	0.383

Note. The P_{KS} and P_{AD} are the probabilities from two-sample KS and AD tests, respectively, that the two distributions being compared (with respective mean values) are drawn from the same parent distribution. For the global distribution of all 109 SNe Ia, the mean values of $\widetilde{R}_{SN} = 0.45 \pm 0.04$ and $\widehat{R}_{SN} = 1.94 \pm 0.18$. For 94 SNe Ia, the mean value of $Fr_g = 0.54 \pm 0.03$. Recall that 15 SNe, which are located far outside the elliptical apertures where fluxes are consistent with the sky background values, are removed from the fractional radial flux analysis (see Section 2).

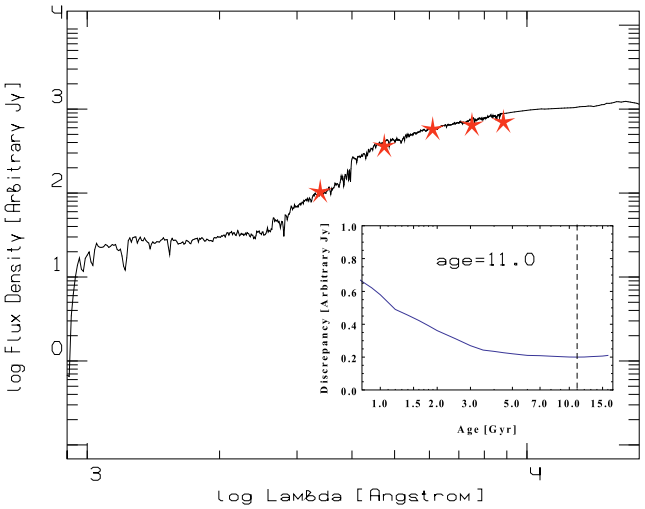

Figure 7. Photometric points (in the SDSS five bands, red asterisks) of SN 2018zs host elliptical galaxy with the best SED, all in the rest frame. The inset shows the curve of the dependence of the model rms deviations on age for the galaxy, with the best age of 11 Gyr (minimum of the curve is shown by the vertical dashed line).

2017, for early-type/high-mass galaxies)

$$\log\left(\frac{Z_*}{Z_\odot}\right) = -1.757 + 0.168 \log\left(\frac{M_*}{M_\odot}\right), \quad (7)$$

where Z_* has solar metallicity units, with a scatter of ∼0.1 dex. It should be noted that we use mass measurements coupled to a (monotonic) formula to convert it to host metallicity, which adds no original information to the statistical analysis, however, this gives a chance to qualitatively discuss our results in term of metallicities of SNe Ia hosts (see Section 4).

Finally, following the procedure outlined in Verkhodanov et al. (2000), we use the fixed redshifts of SN hosts to fit the PEGASE.2 (Fioc & Rocca-Volmerange 1997, 1999) elliptical galaxy models to our *u*-, *g*-, *r*-, *i*-, and *z*-band photometry to determine the luminosity-weighted ages of hosts.[13] In short, the measured five photometric points of a host galaxy in the SDSS bands with fixed redshift are used to select the best location of the points on the spectral energy distribution (SED) templates. Such a location can be found by shifting the points lengthwise and transverse the SED template at which the sum of the squares of the discrepancies is a minimum. From the PEGASE.2 model (Fioc & Rocca-Volmerange 1997, 1999), the procedure uses already computed collection of synthetic SED templates for different ages (up to 19 Gyr) of elliptical galaxies. Fig. 7 presents an example of SN host galaxy photometric points (in the SDSS five bands) with the best SED, all in the rest frame. For more detailed information on the SED fitting procedure with filter smoothing option, the reader is referred to http://sed.sao.ru/.

To reveal possible differences in global properties of SNe Ia elliptical hosts, in Table 6, using the two-sample KS and AD tests, we compare absolute magnitudes, colours, sizes, elongations, stellar masses, average metallicities, and luminosity-weighted ages between the subsamples of host galaxies of normal and 91bg-like SNe. The table shows that the distributions of absolute magnitudes, $g - i$ and $r - z$ colours (red part of the SEDs), sizes, elongations, stellar masses, and average metallicities are not significantly

[13]The luminosity-weighted ages of our 104 elliptical host galaxies are available in the online version (Supporting Information) of this article.

Table 6. Comparison of the distributions of absolute magnitudes, colours, sizes, elongations, stellar masses, average metallicities, and luminosity-weighted ages between the subsamples of host galaxies of normal and 91bg-like SNe.

Parameter	normal	versus	91bg-like	P_{KS}	P_{AD}
	⟨Parameter⟩ ± σ		⟨Parameter⟩ ± σ		
	$\widetilde{R}_{SN} \geq 0$ (66 versus 41 hosts)				
M_u (mag)	-19.6 ± 1.0	versus	-19.8 ± 0.9	0.218	0.276
M_g (mag)	-21.2 ± 1.1	versus	-21.5 ± 0.9	0.112	0.137
M_r (mag)	-22.0 ± 1.1	versus	-22.3 ± 0.9	0.113	0.134
M_i (mag)	-22.4 ± 1.1	versus	-22.7 ± 0.9	0.188	0.153
M_z (mag)	-22.6 ± 1.1	versus	-22.9 ± 0.9	0.260	0.156
$u - r$ (mag)	2.4 ± 0.1	versus	2.5 ± 0.1	**0.013**	**0.007**
$g - i$ (mag)	1.2 ± 0.1	versus	1.2 ± 0.1	0.101	0.255
$r - z$ (mag)	0.7 ± 0.05	versus	0.7 ± 0.04	0.107	0.179
R_{25} (kpc)	23.0 ± 12.6	versus	25.6 ± 11.3	0.096	0.142
R_e (kpc)	6.0 ± 3.8	versus	6.0 ± 3.0	0.296	0.345
a/*b*	1.3 ± 0.2	versus	1.3 ± 0.2	0.766	0.729
$\log(M_*/M_\odot)$	$11.1^{+0.3}_{-1.3}$	versus	$11.2^{+0.2}_{-0.6}$	0.107	0.175
$\log(Z_*/Z_\odot)$	$0.09^{+0.07}_{-0.08}$	versus	$0.11^{+0.06}_{-0.07}$	0.107	0.175
age (Gyr)	$11.7^{+2.3}_{-2.8}$	versus	$12.8^{+1.2}_{-1.6}$	**0.017**	**0.012**
	$\widetilde{R}_{SN} \geq 0.1$ (54 versus 38 hosts)				
M_u (mag)	-19.6 ± 1.0	versus	-19.8 ± 0.8	0.286	0.416
M_g (mag)	-21.2 ± 1.1	versus	-21.4 ± 0.8	0.309	0.275
M_r (mag)	-22.0 ± 1.1	versus	-22.2 ± 0.9	0.306	0.252
M_i (mag)	-22.4 ± 1.1	versus	-22.6 ± 0.9	0.365	0.325
M_z (mag)	-22.7 ± 1.1	versus	-22.9 ± 0.9	0.365	0.314
$u - r$ (mag)	2.4 ± 0.1	versus	2.5 ± 0.1	**0.047**	**0.018**
$g - i$ (mag)	1.2 ± 0.1	versus	1.2 ± 0.1	0.480	0.721
$r - z$ (mag)	0.7 ± 0.05	versus	0.7 ± 0.04	0.274	0.462
R_{25} (kpc)	23.3 ± 12.7	versus	24.2 ± 9.9	0.389	0.399
R_e (kpc)	6.1 ± 4.0	versus	5.5 ± 2.3	0.450	0.390
a/*b*	1.2 ± 0.2	versus	1.3 ± 0.2	0.706	0.559
$\log(M_*/M_\odot)$	$11.2^{+0.3}_{-1.2}$	versus	$11.2^{+0.2}_{-0.5}$	0.224	0.385
$\log(Z_*/Z_\odot)$	$0.09^{+0.07}_{-0.08}$	versus	$0.10^{+0.06}_{-0.06}$	0.224	0.385
age (Gyr)	$11.9^{+2.1}_{-2.7}$	versus	$12.7^{+1.3}_{-1.7}$	**0.025**	**0.032**

Note. The P_{KS} and P_{AD} are the probabilities from two-sample KS and AD tests, respectively, that the two distributions being compared (with respective mean values and standard deviations) are drawn from the same parent distribution. The statistically significant differences (P-values ≤ 0.05) between the distributions are highlighted in bold.

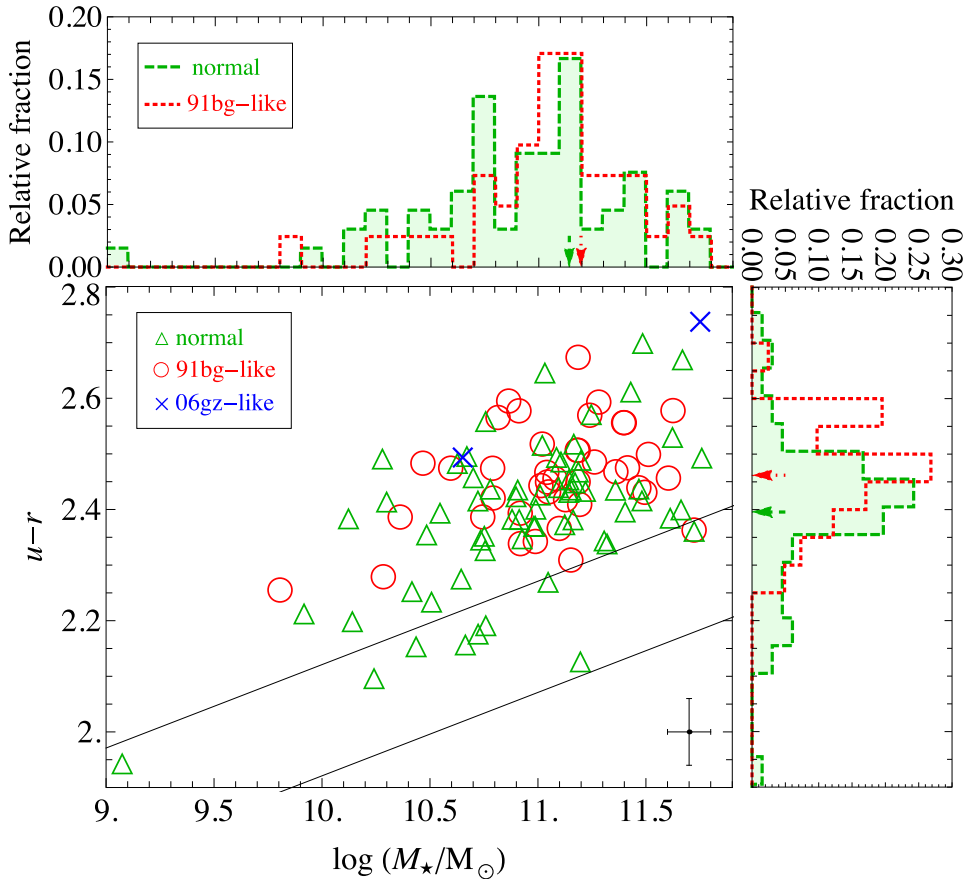

Figure 8. The $u - r$ colour–mass diagram for 109 SNe Ia elliptical host galaxies. Green triangles, red circles, and blue crosses show normal, 91bg-like, and 06gz-like SNe hosts, respectively. The region between two solid lines indicates the Green Valley (see the text for more details). The vertical and horizontal error bars, in the bottom right corner, show the characteristic errors in the colour and mass estimations, respectively. For normal (green dashed and filled) and 91bg-like (red dotted) SNe hosts, the right and upper panels represent separately the histograms of the colours and masses, respectively. The mean values of the distributions are shown by arrows.

different between host galaxies of normal and 91bg-like SNe. On the other hand, the distributions of $u - r$ colours (blue part of the SEDs) and luminosity-weighted ages of the hosts are significantly inconsistent between the subclasses of SNe Ia. In the histograms of Fig. 8, we show the distributions of host galaxy stellar masses and $u - r$ colours. The cumulative distributions of luminosity-weighted ages of the elliptical hosts are presented in Fig. 9. It is clear that, despite their comparable stellar masses, the elliptical host galaxies of normal SNe Ia are on average bluer and younger than those of 91bg-like SNe.

In Table 6, we also check the impact of the described bias in Section 3.2, i.e. the stronger central loss of 91bg-like SNe, on the comparison of the global properties of ellipticals by excluding the host galaxies with $\widetilde{R}_{SN} < 0.1$. We obtain nearly identical results showing that the central bias has negligible impact on the comparison of the elliptical host galaxies in Table 6.

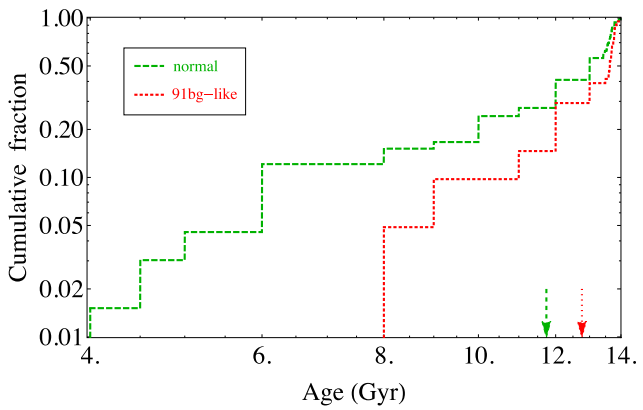

Figure 9. Cumulative distributions of luminosity-weighted ages of elliptical host galaxies of normal (green dashed) and 91bg-like (red dotted) SNe. The mean values of the distributions are shown by arrows.

4 DISCUSSION AND SUMMARY

In this section, we discuss all the results obtained above and give summary within an evolutionary (interacting) scenario of SNe Ia elliptical host galaxies that can explain the similarity of the spatial distributions of normal and 91bg-like SNe in hosts and at the same time the differences of some global properties of elliptical hosts such as the $u - r$ colours and the ages of the stellar population.

In Section 3.2, we have shown that the distributions of projected galactocentric radii (with different normalizations) of normal and

91bg-like SNe in elliptical galaxies follow the de Vaucouleurs model, except in the central region of ellipticals where the different SN surveys are biased against the discovery of the events (Table 3 and Fig. 5). These results are in agreement with a more generalized result of Förster & Schawinski (2008), who showed that the projected surface density distribution of Type Ia SNe (without separating the subclasses) in morphologically selected early-type host galaxies is consistent with the de Vaucouleurs profile (see also Tsvetkov et al. 2004; Dilday et al. 2010). Even without specifying the profile shape and excluding the bias against central SNe, the radial distributions of SN Ia subclasses are consistent with the radial light distribution of stellar populations of elliptical hosts in the SDSS *g*-band (Table 4 and Fig. 6). We have not seen any significant differences between the radial distributions of normal and 91bg-like SNe (Table 5).

These results are in agreement with those of Gallagher et al. (2005), who studied the distribution of 57 local Type Ia SNe LC decline rates (Δm_{15}) in the *B*-band versus projected distances (in kpc) from the centres of spiral and E–S0 host galaxies. Despite their smaller statistics of E–S0 galaxies, they found that the Δm_{15} values are distributed evenly with projected galactocentric radii, showing no preference to the centre of host galaxies for slowly declining (normal SNe Ia) or faster declining (91bg-like) SNe (see also Ivanov et al. 2000, for projected and normalized galactocentric radii). Using a larger SN Ia sample at redshifts below 0.25 and output parameters from two LC fitters, MLCS2k2 (Jha, Riess & Kirshner 2007) and SALT2 (Guy et al. 2007), Galbany et al. (2012) also studied the dependencies between SN properties and the projected galactocentric radii. For 64 SNe Ia in elliptical hosts, with determined morphology based on the concentration indices and Sérsic profiles, the authors found some indications that SNe tend to have faster declining LCs if they explode at larger galactocentric radii. However, this trend is visible when the LC parameters from MLCS2k2 were used, in contrast to the homologous parameters from SALT2. In addition, Galbany et al. noted that their finding might be due to the possible selection effects and explained by the difficulty in detecting faster declining/fainter SNe Ia near the galaxy centre, which we demonstrated in Section 3.2, based on the surface density distributions of normal and 91bg-like events in elliptical hosts.

In Section 3.4, we have shown that the distributions of absolute magnitudes, stellar masses, and average metallicities are not significantly different between host galaxies of normal and 91bg-like SNe (Table 6). Similar results were also obtained by Gallagher et al. (2005), who found no correlation between the LC decline rates of SNe Ia and absolute *B*-band magnitudes (a sufficient tracer of galactic mass) of their E–S0 hosts. Gallagher et al. (2008) also studied optical absorption-line spectra of 29 early-type (mostly E–S0) host galaxies of SNe Ia up to about 200 Mpc and found a mild correlation, if any, between host global metallicity and SN Ia peak luminosity.

Indeed, the variety of metallicities of the main-sequence stars that become WDs could theoretically affect the mass of ^{56}Ni synthesized in SNe Ia (Timmes, Brown & Truran 2003), and cause a variety in the properties of SNe Ia (e.g. in luminosities and/or decline rates). These authors hypothesized that less luminous SNe Ia arise from high-metallicity progenitors that produce less ^{56}Ni. However, Howell et al. (2009) noted that the effect is dominant at metallicities significantly above solar, whereas early-type hosts of SNe Ia have only moderately above solar metallicities (with no detectable star formation). In this respect, our elliptical host galaxies also span moderately above solar metallicities (see Table 6), mostly within $0 \lesssim \log(Z_*/Z_\odot) \lesssim 0.2$ range, and therefore the metallicity effect in our sample might be sufficient to vary the optical peak brightness of SN Ia by less than 0.2 mag (Timmes et al. 2003), but not enough for the differences between peak magnitudes of normal and 91bg-like SNe (as already mentioned, the latter have peak luminosities that are 2 ± 0.5 mag lower in optical bands than do normal SNe, see Taubenberger et al. 2008).

On the other hand, the radial metallicity gradient in elliptical galaxies (e.g. Henry & Worthey 1999) might be a useful tool to probe the differences between the properties of SN Ia subclasses. However, González Delgado et al. (2015) recently studied nearby galaxies, including 41 ellipticals, with redshifts < 0.03, using the precise data of integral field spectroscopy, and found that the average radial metallicity profile of elliptical galaxies (with negative gradient) declines only moderately from 0.2 dex above solar to solar from the galactic centre up to $3R_e$, respectively. Therefore, most probably this small metallicity variation does not allow (according to Timmes et al. 2003) to see the differences between the distributions of normal and 91bg-like SNe along the radius of their elliptical hosts (Table 5). Our results confirm that the masses as well as global and radial metallicity distributions of elliptical hosts are not decisive factors of the nature of normal and 91bg-like SN populations (see also discussions by Ivanov et al. 2000; Gallagher et al. 2005, 2008).

At the same time, in Section 3.4, we have shown that the distributions of $u - r$ colours and luminosity-weighted ages are inconsistent significantly between the elliptical host galaxies of different SN Ia subclasses (Table 6): the hosts of normal SNe Ia are on average bluer (the right histograms in Fig. 8) and younger (Fig. 9) than those of 91bg-like SNe. These results are in excellent agreement with those of Gallagher et al. (2008), who found a strong correlation between SN peak luminosities and the luminosity-weighted ages of dominant population of E–S0 hosts. They suggested that SNe Ia in galaxies with a characteristic age greater than several Gyr are on average $\sim$1 mag fainter at the peak in *V*-band than those in early-type hosts with younger populations (i.e. a fairly large number of subluminous/91bg-like SNe are discovered in older hosts). In addition, Gallagher et al. (2008) noted about the difficulty to distinguish whether this effect is a smooth transition with age or the result of two distinct SN Ia populations. Most recently, Panther et al. (2019) analysed integral field observations of the apparent/underlying explosion sites of 11 spectroscopically identified 91bg-like SNe (redshifts ≤ 0.04) in hosts with different morphologies (including six E–S0 galaxies) and found that the majority of the stellar populations that host these events are dominated by old stars with a lack of evidence for recent star formation. Panther et al. concluded that the 91bg-like SN progenitors are likely to have delay time distribution weighted towards long delay times (>6 Gyr, see also Crocker et al. 2017), much longer than the typical delay times of normal SNe Ia in star-forming environments, whose delay times peak between several hundred Myr and $\sim$1 Gyr (e.g. Childress et al. 2014; Maoz et al. 2014). These results are in good agreement with our findings in Table 6 and Fig. 9.

It is important to note that the global ages of elliptical galaxies are not significantly different, on average, from local ones at any radii, i.e. there is no clear age gradient in ellipticals, being only mildly negative up to R_e and flat beyond that radius (e.g. González Delgado et al. 2015). For this reason, we see no difference between the radial distributions of the subclasses of SNe Ia (Table 5), meanwhile seeing the clear differences of the global ages of normal and 91bg-like hosts (Table 6 and Fig. 9). Thus, our results support the earlier suggestions (e.g. Ivanov et al. 2000; Gallagher et al. 2005, 2008; Kang et al. 2016) that the age of SN Ia progenitor populations is a more

important factor than metallicity or mass of elliptical host galaxies in determining the properties of normal and 91bg-like events.

We now interpret and summarize our results within an evolutionary (interacting) scenario of SNe Ia elliptical host galaxies. In Fig. 8, we show $u - r$ colour–mass diagram of elliptical host galaxies (the right-hand and upper panels represent separately the histograms of the colours and masses, respectively). In Fig. 8, the region between two solid lines indicates the location of the Green Valley, i.e. the region between blue star-forming galaxies and the red sequence of quiescent E–S0 galaxies (e.g. Mendez et al. 2011; Schawinski et al. 2014). For galaxies with elliptical morphology, this is a transitional state through which blue galaxies evolve into the red sequence via major merging processes with morphological transformation from disc to spheroidal shape (e.g. Schawinski et al. 2010; McIntosh et al. 2014), and/or a state of galaxies demonstrating some residual star formation via minor merging processes with no global changes in spheroidal structure (e.g. Kaviraj et al. 2009).

It should be noted that we use the modification of the Green Valley defined by Schawinski et al. (2014). These authors used the SDSS `modelMag` values[14] of about 9000 early- and about 17 000 late-type galaxies with redshifts $0.02 < z < 0.05$, while we use the magnitudes of host galaxies based on the g-band 25 mag arcsec^{-2} elliptical apertures (see Section 2). The comparison of SDSS DR15 `modelMag` measurements of our elliptical host galaxies with those obtained in Section 2, and the best fit of our $u - r$ versus $\log(M_*/\mathrm{M}_\odot)$ bring a negative shift and a small change in slope for the modification of the Green Valley[15] in comparison with that in Schawinski et al. (2014).

In Fig. 8, we see that the tail of the colour distribution of normal SN hosts stretches well into the Green Valley, while the same tail of 91bg-like SN hosts barely reaches the Green Valley border, and only at high stellar masses. To quantify this difference, we compare the distributions of colour residuals of elliptical hosts of the SN subclasses relative to the upper border of our Green Valley (see Fig. 10). The two-sample KS and AD tests show that the distributions are significantly different ($P_{\mathrm{KS}} = 0.049, P_{\mathrm{AD}} = 0.026$). Therefore, the bluer and younger elliptical hosts of normal SNe Ia should have more residual star formation (e.g. Kaviraj et al. 2009; Schawinski et al. 2014) that gives rise to younger SN Ia progenitors, resulting in normal SNe with shorter delay times (e.g. Childress, Wolf & Zahid 2014; Maoz, Mannucci & Nelemans 2014; Uddin, Mould & Wang 2017). Interestingly, the results of Gomes et al. (2016a,b) reveal that in such galaxies the residual star formation is well mixed radially and distributed within entire stellar population.

As was recalled in the Introduction, the rate of SNe Ia can be represented as a linear combination of prompt and delayed components (e.g. Scannapieco & Bildsten 2005). The prompt component is dependent on the rate of recent star formation, and the delayed component is dependent on the galaxy total stellar mass (e.g. Mannucci et al. 2005; Hakobyan et al. 2011; Li et al. 2011b). In this context, the normal SNe Ia with shorter delay times correspond to the prompt component. The bluer and younger ellipticals (with residual star formation) can also produce 91bg-like events with

[14]The `modelMag` values are first calculated using the best-fitting parameters in the r-band, and then applied these parameters to all other SDSS bands, therefore, the light is measured consistently through the same aperture in all bands.

[15]The best fit is $u - r = 0.721 + 0.155\ \log(M_*/\mathrm{M}_\odot)$ for normal and 91bg-like SNe hosts. The upper and bottom borders of our Green Valley in Fig. 8 are simply negative shifts of the best fit in 0.1 and 0.3 mag, respectively.

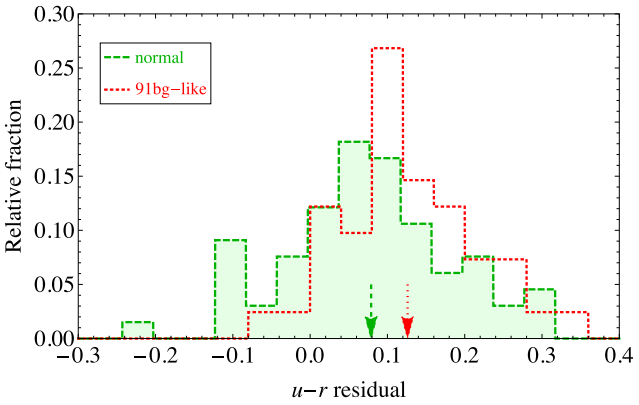

Figure 10. Distributions of colour residuals of elliptical hosts of normal (green dashed and filled) and 91bg-like (red dotted) SNe relative to the upper border of our Green Valley. The mean values of the distributions are shown by arrows.

lower rate (e.g. Gallagher et al. 2008), because of long delay times of these SNe (e.g. Panther et al. 2019), i.e. a delayed component of SN Ia explosions (e.g. Scannapieco & Bildsten 2005; González-Gaitán et al. 2011). However, the distribution of host ages (lower age limit of the delay times) of 91bg-like SNe does not extend down to the stellar ages that produce a significant excess of $u - r$ colour (i.e. u-band flux, see Figs 8 and 9) – younger stars in elliptical hosts do not produce 91bg-like SNe, i.e. the 91bg-like events have no prompt component. The redder and older elliptical hosts that already exhausted nearly all star formation budget during the evolution (e.g. Schawinski et al. 2014) may produce significantly less normal SNe Ia with shorter delay times, outnumbered by 91bg-like SNe with long delay times.

Finally, we would like to note that our results favour SN Ia progenitor models such as helium-ignited violent mergers as a unified model for normal (CO WD primary with CO WD companion) and 91bg-like (CO WD primary with He WD companion) SNe (e.g. Pakmor et al. 2013; Crocker et al. 2017) that have the potential to explain the different luminosities, delay times, and relative rates of the SN subclasses (see also Gilfanov & Bogdán 2010; Lipunov, Panchenko & Pruzhinskaya 2011, for discussions of binary WDs mergers in elliptical galaxies). In particular, the models predict shorter delay times for normal SNe Ia in agreement with our finding that normal SNe occur in younger stellar population of elliptical hosts. Moreover, the model prediction of very long delay times for 91bg-like SNe ($\gtrsim$ several Gyr, Crocker et al. 2017) is in good qualitative agreement with our estimation of older ages of host galaxies of these events.

In the years of the surveys by robotic telescopes on different sites on the globe (e.g. All Sky Automated Survey for SuperNovae; Kochanek et al. 2017) and of the forthcoming Large Synoptic Survey Telescope (Tyson 2002), thousands of relatively nearby SNe Ia with spectroscopic confirmations are expected to be discovered that will provide larger and better defined samples of these transient events. We will then be able to place tighter constraints on the evolutionary scenarios of host galaxies and on the photometric and spectroscopic properties of Type Ia SNe with different progenitor models.

ACKNOWLEDGEMENTS

We would like to thank the referee, Michael Childress, for excellent comments that improved the clarity of this paper. LVB,

AAH, and AGK acknowledge the hospitality of the Institut d'Astrophysique de Paris (France) during their stay as visiting scientists supported by the Programme Visiteurs Extérieurs (PVE). This work was supported by the RA MES State Committee of Science, in the frames of the research project number 15T–1C129. This work was made possible in part by a research grant from the Armenian National Science and Education Fund (ANSEF) based in New York, USA. VA acknowledges the support from Fundação para a Ciência e Tecnologia (FCT) through Investigador FCT contract nr. IF/00650/2015/CP1273/CT0001 and the support from FCT/MCTES through national funds (PIDDAC) – UID/FIS/04434/2019. Funding for the SDSS-IV has been provided by the Alfred P. Sloan Foundation, the US Department of Energy Office of Science, and the Participating Institutions. SDSS-IV acknowledges support and resources from the Center for High-Performance Computing at the University of Utah. The SDSS web site is www.sdss.org. SDSS-IV is managed by the Astrophysical Research Consortium for the Participating Institutions of the SDSS Collaboration including the Brazilian Participation Group, the Carnegie Institution for Science, Carnegie Mellon University, the Chilean Participation Group, the French Participation Group, Harvard-Smithsonian Center for Astrophysics, Instituto de Astrofísica de Canarias, The Johns Hopkins University, Kavli Institute for the Physics and Mathematics of the Universe (IPMU) / University of Tokyo, the Korean Participation Group, Lawrence Berkeley National Laboratory, Leibniz Institut für Astrophysik Potsdam (AIP), Max-Planck-Institut für Astronomie (MPIA Heidelberg), Max-Planck-Institut für Astrophysik (MPA Garching), Max-Planck-Institut für Extraterrestrische Physik (MPE), National Astronomical Observatories of China, New Mexico State University, New York University, University of Notre Dame, Observatário Nacional / MCTI, The Ohio State University, Pennsylvania State University, Shanghai Astronomical Observatory, United Kingdom Participation Group, Universidad Nacional Autónoma de México, University of Arizona, University of Colorado Boulder, University of Oxford, University of Portsmouth, University of Utah, University of Virginia, University of Washington, University of Wisconsin, Vanderbilt University, and Yale University.

REFERENCES

Aguado D. S. et al., 2019, ApJS, 240, 23
Anderson J. P., James P. A., 2009, MNRAS, 399, 559
Anderson J. P., James P. A., Förster F., González-Gaitán S., Habergham S. M., Hamuy M., Lyman J. D., 2015, MNRAS, 448, 732
Aramyan L. S. et al., 2016, MNRAS, 459, 3130
Arnett W. D., 1982, ApJ, 253, 785
Barbon R., Buondí V., Cappellaro E., Turatto M., 1999, A&AS, 139, 531
Bartunov O. S., Makarova I. N., Tsvetkov D. I., 1992, A&A, 264, 428
Benetti S. et al., 2005, ApJ, 623, 1011
Bernardi M., Nichol R. C., Sheth R. K., Miller C. J., Brinkmann J., 2006, AJ, 131, 1288
Bottinelli L., Gouguenheim L., Paturel G., Teerikorpi P., 1995, A&A, 296, 64
Branch D., Fisher A., Nugent P., 1993, AJ, 106, 2383
Capaccioli M., 1989, in Corwin H. G. Jr, Bottinelli L., eds, The World of Galaxies. Springer-Verlag, New York, p. 208
Cappellaro E., Turatto M., 1997, in Ruiz-Lapuente P., Canal R., Isern J., eds, NATO Adv. Sci. Inst. Ser. C, Vol. 486 , Thermonuclear Supernovae. Springer, Dordrecht, p. 77
Chen Y.-M. et al., 2012, MNRAS, 421, 314
Childress M. J., Wolf C., Zahid H. J., 2014, MNRAS, 445, 1898
Conroy C., Gunn J. E., White M., 2009, ApJ, 699, 486
Crocker R. M. et al., 2017, Nat. Astron., 1, 0135
D'Agostino R. B., Stephens M. A., 1986, Statistics: Textbooks and Monographs, Vol. 68. Marcel Dekker Inc., New York
de Vaucouleurs G., 1948, Ann. Astrophys., 11, 247
Dilday B. et al., 2010, ApJ, 715, 1021
Dong S., Katz B., Kushnir D., Prieto J. L., 2015, MNRAS, 454, L61
Engmann S., Cousineau D., 2011, J. Appl. Quant. Methods, 6, 1
Filippenko A. V. et al., 1992a, AJ, 104, 1543
Filippenko A. V. et al., 1992b, ApJ, 384, L15
Fioc M., Rocca-Volmerange B., 1997, A&A, 326, 950
Fioc M., Rocca-Volmerange B., 1999, preprint (arXiv:astro-ph/9912179)
Förster F., Schawinski K., 2008, MNRAS, 388, L74
Freeman K. C., 1970, ApJ, 160, 811
Galbany L. et al., 2012, ApJ, 755, 125
Gallagher J. S., Garnavich P. M., Berlind P., Challis P., Jha S., Kirshner R. P., 2005, ApJ, 634, 210
Gallagher J. S., Garnavich P. M., Caldwell N., Kirshner R. P., Jha S. W., Li W., Ganeshalingam M., Filippenko A. V., 2008, ApJ, 685, 752
Gallazzi A., Charlot S., Brinchmann J., White S. D. M., 2006, MNRAS, 370, 1106
Gilfanov M., Bogdán Á., 2010, Nature, 463, 924
Gomes J. M. et al., 2016a, A&A, 585, A92
Gomes J. M. et al., 2016b, A&A, 588, A68
González Delgado R. M. et al., 2015, A&A, 581, A103
González-Gaitán S. et al., 2011, ApJ, 727, 107
González-Gaitán S. et al., 2014, ApJ, 795, 142
Guillochon J., Parrent J., Kelley L. Z., Margutti R., 2017, ApJ, 835, 64
Gupta R. R. et al., 2011, ApJ, 740, 92
Guseinov O. H., Kasumov F. K., Kalinin E. V., 1980, Ap&SS, 68, 385
Guy J. et al., 2007, A&A, 466, 11
Hakobyan A. A. et al., 2011, Astrophysics, 54, 301
Hakobyan A. A., Adibekyan V. Z., Aramyan L. S., Petrosian A. R., Gomes J. M., Mamon G. A., Kunth D., Turatto M., 2012, A&A, 544, A81
Hakobyan A. A. et al., 2014, MNRAS, 444, 2428
Hakobyan A. A. et al., 2016, MNRAS, 456, 2848
Hakobyan A. A. et al., 2017, MNRAS, 471, 1390
Hamuy M., Pinto P. A., 1999, AJ, 117, 1185
Hamuy M., Phillips M. M., Suntzeff N. B., Schommer R. A., Maza J., Aviles R., 1996, AJ, 112, 2391
Hamuy M., Trager S. C., Pinto P. A., Phillips M. M., Schommer R. A., Ivanov V., Suntzeff N. B., 2000, AJ, 120, 1479
Henry R. B. C., Worthey G., 1999, PASP, 111, 919
Hillebrandt W., Niemeyer J. C., 2000, ARA&A, 38, 191
Howell D. A., 2001, ApJ, 554, L193
Howell D. A., Wang L., Wheeler J. C., 2000, ApJ, 530, 166
Howell D. A. et al., 2009, ApJ, 691, 661
Iben I. Jr, Tutukov A. V., 1984, ApJS, 54, 335
Ivanov V. D., Hamuy M., Pinto P. A., 2000, ApJ, 542, 588
James P. A., Anderson J. P., 2006, A&A, 453, 57
Jha S., Riess A. G., Kirshner R. P., 2007, ApJ, 659, 122
Kang Y., Kim Y.-L., Lim D., Chung C., Lee Y.-W., 2016, ApJS, 223, 7
Kaviraj S., Peirani S., Khochfar S., Silk J., Kay S., 2009, MNRAS, 394, 1713
Kim Y.-L., Smith M., Sullivan M., Lee Y.-W., 2018, ApJ, 854, 24
Kochanek C. S. et al., 2017, PASP, 129, 104502
Kollmeier J. A. et al., 2019, MNRAS, 486, 3041
Kormendy J., Fisher D. B., Cornell M. E., Bender R., 2009, ApJS, 182, 216
Leaman J., Li W., Chornock R., Filippenko A. V., 2011, MNRAS, 412, 1419
Leibundgut B. et al., 1993, AJ, 105, 301
Li W. et al., 2011a, MNRAS, 412, 1441
Li W., Chornock R., Leaman J., Filippenko A. V., Poznanski D., Wang X., Ganeshalingam M., Mannucci F., 2011b, MNRAS, 412, 1473
Lipunov V. M., Panchenko I. E., Pruzhinskaya M. V., 2011, New A, 16, 250
Lupton R., Gunn J. E., Ivezić Z., Knapp G. R., Kent S., 2001, in Harnden F. R. Jr, Primini F. A., Payne H. E., eds, ASP Conf. Ser. Vol. 238, Astronomical Data Analysis Software and Systems X. Astron. Soc. Pac., San Francisco, p. 269
Maeda K., Terada Y., 2016, Int. J. Mod. Phys. D, 25, 1630024

Mannucci F., Della Valle M., Panagia N., Cappellaro E., Cresci G., Maiolino R., Petrosian A., Turatto M., 2005, A&A, 433, 807
Maoz D., Mannucci F., Nelemans G., 2014, ARA&A, 52, 107
Maraston C., 2005, MNRAS, 362, 799
Massey F. J., 1951, J. Am. Stat. Assoc., 46, 68
Maza J., van den Bergh S., 1976, ApJ, 204, 519
Mazzali P. A., Hachinger S., 2012, MNRAS, 424, 2926
Mazzali P. A., Röpke F. K., Benetti S., Hillebrandt W., 2007, Science, 315, 825
McIntosh D. H. et al., 2014, MNRAS, 442, 533
Mendez A. J., Coil A. L., Lotz J., Salim S., Moustakas J., Simard L., 2011, ApJ, 736, 110
Moreno-Raya M. E., López-Sánchez Á. R., Mollá M., Galbany L., Vílchez J. M., Carnero A., 2016, MNRAS, 462, 1281
Nair P. B., Abraham R. G., 2010, ApJS, 186, 427
Neill J. D. et al., 2009, ApJ, 707, 1449
Nomoto K., Iwamoto K., Kishimoto N., 1997, Science, 276, 1378
Pakmor R., Kromer M., Taubenberger S., Springel V., 2013, ApJ, 770, L8
Pan Y.-C. et al., 2014, MNRAS, 438, 1391
Pan Y.-C., Sullivan M., Maguire K., Gal-Yam A., Hook I. M., Howell D. A., Nugent P. E., Mazzali P. A., 2015, MNRAS, 446, 354
Panther F. H., Seitenzahl I. R., Ruiter A. J., Crocker R. M., Lidman C., Wang E. X., Tucker B. E., Groves B., 2019, Publ. Astron. Soc. Aust., 36, e031
Pavlyuk N. N., Tsvetkov D. Y., 2016, Astron. Lett., 42, 495
Perlmutter S. et al., 1999, ApJ, 517, 565
Pettitt A. N., 1976, Biometrika, 63, 161
Phillips M. M., 1993, ApJ, 413, L105
Phillips M. M., Wells L. A., Suntzeff N. B., Hamuy M., Leibundgut B., Kirshner R. P., Foltz C. B., 1992, AJ, 103, 1632
Phillips M. M., Lira P., Suntzeff N. B., Schommer R. A., Hamuy M., Maza J., 1999, AJ, 118, 1766
Pskovskii I. P., 1977, SvA, 21, 675
Riess A. G. et al., 1998, AJ, 116, 1009
Rose B. M., Garnavich P. M., Berg M. A., 2019, ApJ, 874, 32
Ruiz-Lapuente P., Cappellaro E., Turatto M., Gouiffes C., Danziger I. J., della Valle M., Lucy L. B., 1992, ApJ, 387, L33
Rust B. W., 1974, PhD thesis, Oak Ridge National Laboratory
Sand D. J. et al., 2019, ApJ, 877, L4
Scannapieco E., Bildsten L., 2005, ApJ, 629, L85
Schawinski K., Dowlin N., Thomas D., Urry C. M., Edmondson E., 2010, ApJ, 714, L108
Schawinski K. et al., 2014, MNRAS, 440, 889
Schlafly E. F., Finkbeiner D. P., 2011, ApJ, 737, 103
Schlegel D. J., Finkbeiner D. P., Davis M., 1998, ApJ, 500, 525
Scott N. et al., 2017, MNRAS, 472, 2833
Sérsic J. L., 1963, Bol. Asoc. Argent. Astron., 6, 41
Shaw R. L., 1979, A&A, 76, 188
Silverman J. M. et al., 2012, MNRAS, 425, 1789
Sullivan M. et al., 2010, MNRAS, 406, 782
Taubenberger S., 2017, in Alsabti A. W., Murdin P., eds, Handbook of Supernovae. Springer, Cham, p. 317
Taubenberger S. et al., 2008, MNRAS, 385, 75
Taubenberger S. et al., 2011, MNRAS, 412, 2735
Taylor E. N. et al., 2011, MNRAS, 418, 1587
Terry J. N., Paturel G., Ekholm T., 2002, A&A, 393, 57
Theureau G., Rauzy S., Bottinelli L., Gouguenheim L., 1998, A&A, 340, 21
Timmes F. X., Brown E. F., Truran J. W., 2003, ApJ, 590, L83
Tomasella L. et al., 2014, Astron. Nachr., 335, 841
Tsvetkov D. Y., Pavlyuk N. N., Bartunov O. S., 2004, Astron. Lett., 30, 729
Turatto M., Benetti S., Cappellaro E., Danziger I. J., Della Valle M., Gouiffes C., Mazzali P. A., Patat F., 1996, MNRAS, 283, 1
Tyson J. A., 2002, in Tyson J. A., Wolff S., eds, Proc. SPIE Conf. Ser. Vol. 4836, Survey and Other Telescope Technologies and Discoveries. SPIE, Bellingham, p. 10
Uddin S. A., Mould J., Wang L., 2017, ApJ, 850, 135
Verkhodanov O. V., Kopylov A. I., Zhelenkova O. P., Verkhodanova N. V., Chernenkov V. N., Parijskij Y. N., Soboleva N. S., Temirova A. V., 2000, Astron. Astrophys. Trans., 19, 662
Vika M., Bamford S. P., Häußler B., Rojas A. L., Borch A., Nichol R. C., 2013, MNRAS, 435, 623
Wang X., Wang L., Filippenko A. V., Zhang T., Zhao X., 2013, Science, 340, 170
Yahil A., Tammann G. A., Sandage A., 1977, ApJ, 217, 903
Yaron O., Gal-Yam A., 2012, PASP, 124, 668

SUPPORTING INFORMATION

Supplementary data are available at *MNRAS* online.

PaperVIonlinedata.csv

Please note: Oxford University Press is not responsible for the content or functionality of any supporting materials supplied by the authors. Any queries (other than missing material) should be directed to the corresponding author for the article.

This paper has been typeset from a TEX/LATEX file prepared by the author.